NASA Contractor Report 186031

In-Flight Imaging of Transverse Gas Jets Injected Into Transonic and Supersonic Crossflows: Design and Development

Kon-Sheng Charles Wang
University of California, Los Angeles
Los Angeles, California

1994

National Aeronautics and
Space Administration

Dryden Flight Research Center
Edwards, California 93523-0273

TABLE OF CONTENTS

LIST OF FIGURES

ABSTRACT

The design and development of an airborne flight-test experiment to study nonreacting gas jets injected transversely into transonic and supersonic crossflows is presented. Free-stream/crossflow Mach numbers range from 0.8 to 2.0. Planar laser-induced fluorescence (PLIF) of an iodine-seeded nitrogen jet is used to visualize the jet flow. Time-dependent images are obtained with a high-speed intensified video camera synchronized to the laser pulse rate. The entire experimental assembly is configured compactly inside a unique flight-test-fixture (FTF) mounted under the fuselage of the F-104G research aircraft, which serves as a "flying wind tunnel" at NASA Dryden Flight Research Center. The aircraft is flown at predetermined speeds and altitudes to permit a perfectly expanded (or slightly underexpanded) gas jet to form just outside the FTF at each free-stream Mach number. Recorded gas jet images are then digitized to allow analysis of jet trajectory, spreading, and mixing characteristics. Comparisons will be made with analytical and numerical predictions. (Results presented in AIAA CP-95-0516). This study shows the viability of applying highly sophisticated ground-based flow diagnostic techniques to flight-test vehicle platforms that can achieve a wide range of thermo/fluid dynamic conditions. Realistic flow environments, high enthalpies, unconstrained flowfields, and moderate operating costs are also realized, in contrast to traditional wind-tunnel testing.

NOMENCLATURE

Roman letters

a	speed of sound
A	area
c_p	specific heat at constant pressure
D	diameter of orifice
$\dot{m}$	mass flow rate
M	Mach number
M_n	Mach number normal to shock wave
p	pressure
q	heat flux per unit area; power
Q	jet-to-free-stream dynamic pressure ratio
R	universal gas constant
T	temperature
U	velocity
v	velocity
X	X-position
Y	Y-position
Z	Z-position

Greek letters

α	angle of attack
β	angle of oblique shock
γ	ratio of specific heats
ν	Prandtl-Meyer function
ρ	density
θ	angle of deflection

Subscripts

1	upstream conditions
2	downstream conditions
0	stagnation/reservoir conditions
jet	jet conditions at exit
exit	exit conditions (interchangeable with jet conditions)
∞	free-stream conditions

CHAPTER I
INTRODUCTION

The development of supersonic and hypersonic flight vehicles capable of atmospheric cruise has been of great interest over the past decade. The high-speed civil transport (HSCT) has been the focus for civilian use, and the national aerospace plane (NASP) has led the way in fundamental aeronautics research. From the point of view of the propulsion system, the scramjet (supersonic combustion ramjet) engine has been proposed for use when the flight Mach numbers exceed 6. Among the difficulties limiting development of the scramjet is an inability to fully understand and predict the nature of the supersonic combustion process. In particular, an understanding is sought for a combustor environment in which very high temperatures and flow velocities, along with complex shock structures, dominate the flowfield. To this end, experimental and computational research in supersonic combustor development has experienced a resurgence over the past several years [Northam and Anderson (1986), Uenishi and Rogers (1986), Reider (1986), ASME Staff Report (1986), Schetz and Billig (1987), Chitsomboon et al. (1988)].

I.1 Background

Transverse injection of hydrogen fuel into a supersonic crossflow of air (Figure 1.1) is the typical flow scenario in the scramjet [McDaniel and Graves (1988), King et al. (1991)]. Experimental studies have utilized conventional mass sampling, schlieren, and shadowgraph techniques as well as modern laser-based imaging techniques such as Rayleigh/Mie scattering and planar laser-induced fluorescence (PLIF) [Lee et al. (1992)]. Analytical and numerical models have also been developed to describe the transverse jet problem. Those developed at UCLA by Karagozian (1986) and Heister and Karagozian (1990ab) are analytically oriented, and emphasize the vortical structures observed to dominate the cross-section of transverse jets injected into a crossflow of the same phase, whether compressible, subsonic, or supersonic; see Figure 1.2. The same counter-rotating, vortex pair structure is also postulated to occur in liquid jets injected into a gaseous crossflow [Heister et al. (1989), Nguyen and Karagozian (1991)]. Previous related studies have been performed by Broadwell and Breidenthal (1984), Kamotani and Greber (1972), and Zukoski and Spaid (1964). The transverse jet is a classical problem in fluid mechanics, whose applications also include fuel jets for conventional turbojet and ramjet combustors, dilutions jets for local cooling processes, thrust vector control systems, and vertical or short takeoff and landing aircraft.

Limited experimental data are available with which numerically predicted trajectories and mixing patterns can be compared. The only datasets for trajectories of gas jets in a supersonic crossflow are those obtained by Lee et al. (1992), McDaniel and Graves (1988), Orth et al. (1969), and Zukoski and Spaid (1964). Data for supersonic jets injected into a subsonic crossflow have been reported for free-stream Mach numbers of 0.6 and 0.8 [Manela and Seginer (1986)]. As indicated in Figure 1.3, the UCLA model by Heister and Karagozian (1990ab) shows reasonably good agreement under both conditions (within 10 percent). Almost all of the supersonic data available is for large free-stream Mach numbers $(2.0 \leq M_\infty \leq 2.5)$, the only exception being a couple of points at $M_\infty = 1.4$ [Lee et al.
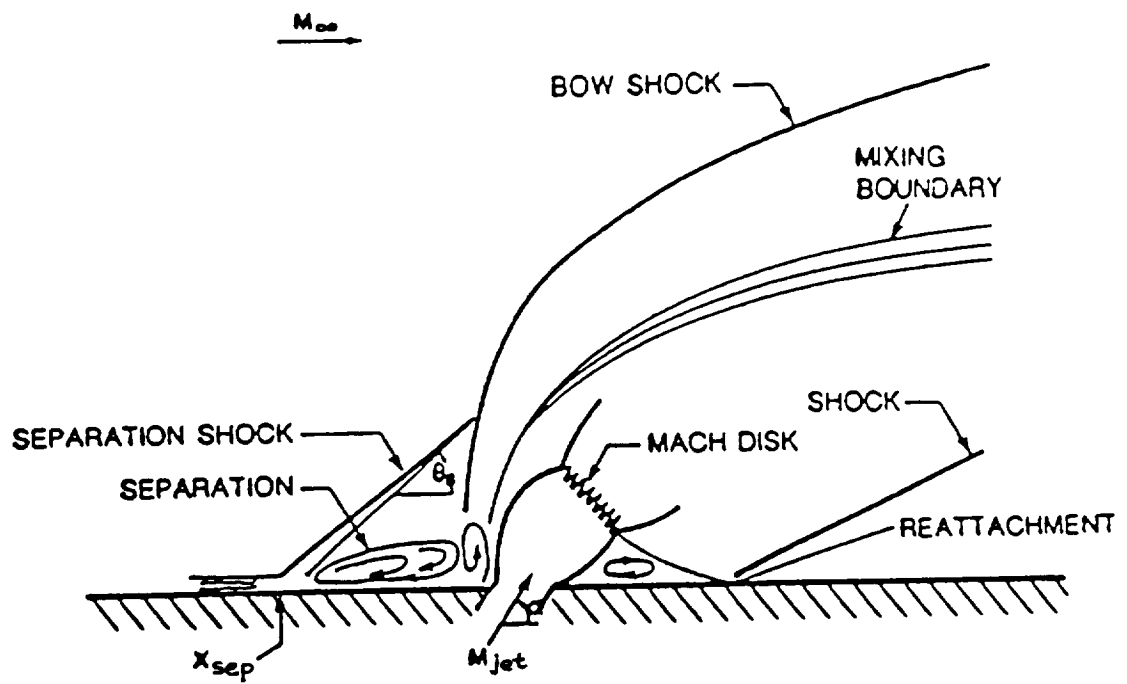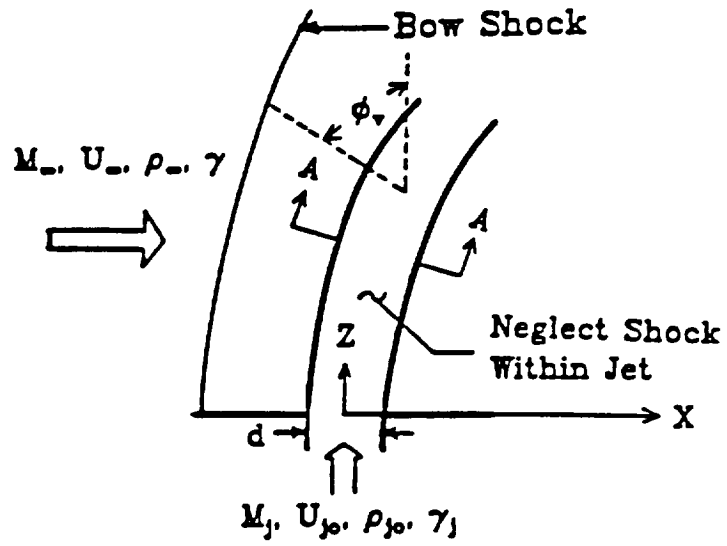
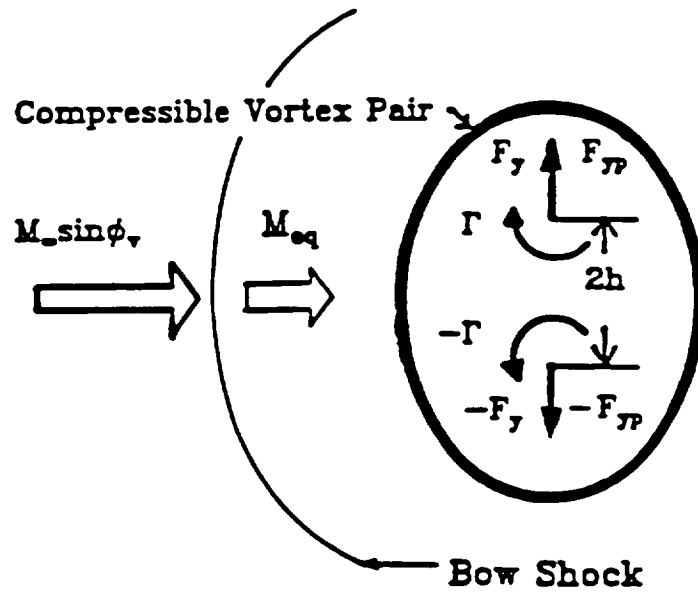Figure 1.1 Fluid Dynamics of Gaseous Transverse Jet Injection

Section A–A

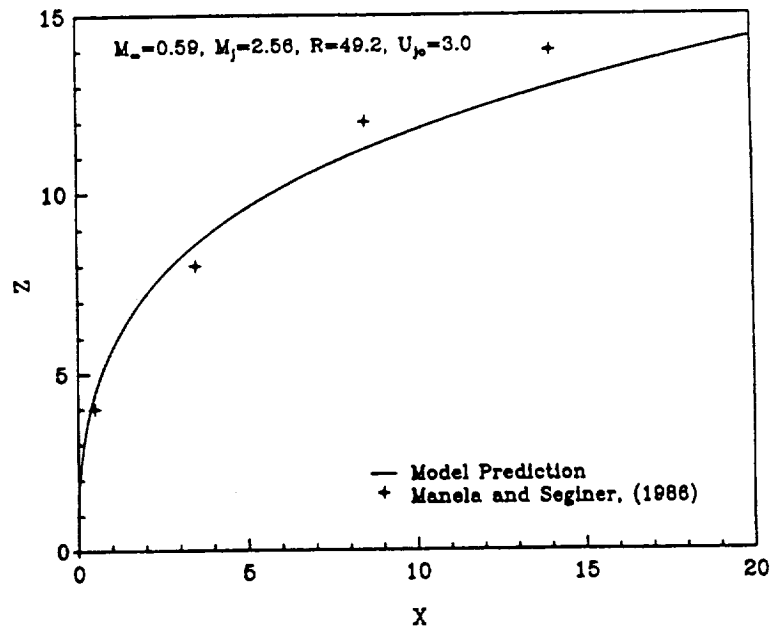Figure 1.2 Heister-Karagozian (1990a) Transverse Jet Model
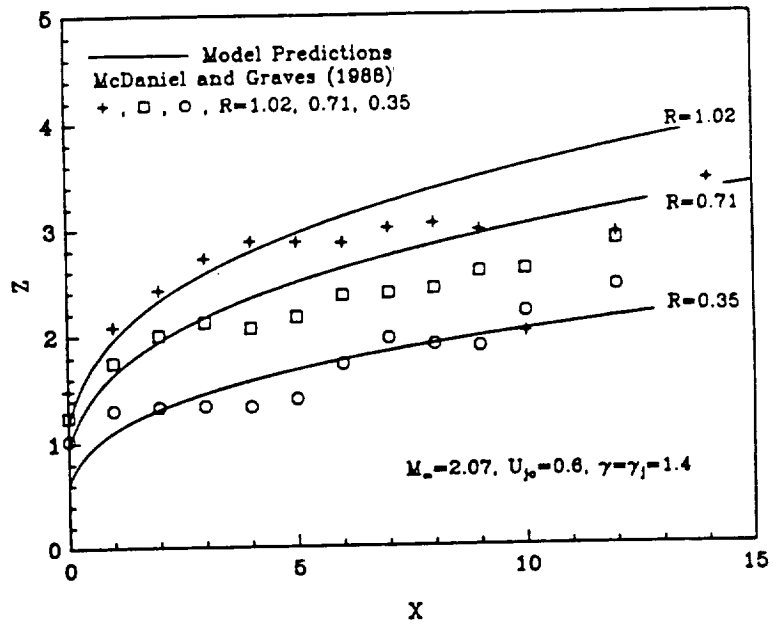
Figure 1.3 Typical Transverse Jet Trajectory Data (supersonic and subsonic)

(1992)] and 1.38 [Orth et al. (1969)]. No data at all are available in the transonic and low supersonic regime $(0.8 < M_\infty < 1.38)$. Because the analytical models behave nonlinearly near M = 1, this regime provides a critical test. In addition, much of the data (as in Zukoski and Spaid (1964)) is for severely underexpanded jets. The models predict increased penetration for perfectly expanded jets, so this should be a more desirable operating condition in a scramjet. Finally, in some cases the wind tunnel data show signs of interference by the tunnel wall in the far field. This is thought to be responsible for the poorer agreement for the jet origin exhibited in Figure 1.3a. In light of these issues, one is motivated to look more extensively at perfectly expanded gas jets in the range $0.8 < M_\infty < 2.0$, and to do so in such a manner that the jet is unconstrained by interaction with the opposing wall.

I.2 Overview

We will examine the flow characteristics of nonreacting transverse gas jets as a function of the jet-to-free-stream momentum flux ratio. For an ideal gas, this is equivalent to the jet-to-free-stream dynamic pressure ratio, or "Q-ratio," and is expressed as:

$$Q = \frac{\frac{\gamma_{jet}}{2} P_{jet} M_{jet}^2}{\frac{\gamma_\infty}{2} P_\infty M_\infty^2}$$

(1.1)

Since our aim is to study perfectly expanded jets (or slightly underexpanded jets), the pressure values in the Q-ratio effectively cancel so that we only need to control jet and free-stream Mach numbers. The ratios of specific heats are approximately the same. In the current phase of our experiments, the jet velocity is fixed at M = 1 (a sonic gas jet), while the free-stream velocity is varied from M = 0.8 to M = 2.0 in increments of 0.2. Thus, we will test Q-ratios: 1.56, 1.00, 0.69, 0.51, 0.39, 0.31, and 0.25. In a future phase, jet velocity will also be varied. The flow characteristics we will be interested in are the jet trajectory (injectant penetration height vs. downstream distance), spreading rates, and mixing rates with the free stream. Special attention will be given to free-stream Mach numbers around M = 1 since, as mentioned above, this region is of special theoretical (and potentially practical) interest. These observations would constitute the first experimental data in this region ever obtained.

Experimental fluid mechanics investigations are typically conducted in ground-based wind tunnel facilities, as surveyed by Pirrello et al. (1971). However, wind tunnel facilities often impose certain limitations on the scope, accuracy, and reliability of the experiments. For example: scale effects due to unit Reynolds number, size limitations for models or test equipment due to test section dimensions, improper scaling of noise or turbulence levels in the wind tunnel, and unreliable data near Mach 1.0 due to problems such as shocks reflected off adjacent and opposing tunnel walls. Another limiting factor in ground facilities is the need to conduct tests in several wind tunnels to span a wide range of Mach numbers. In certain cases, conducting the investigation in flight using the "flying

wind tunnel" concept, wherein an aircraft is used as a carrier vehicle for the experiment, can avoid some or all of the above noted wind tunnel limitations, while maintaining operational costs that are competitive with those of wind tunnels.

For reasonable jet diameters to be used in our experiments, it would indeed be very expensive to conduct tests in a large enough wind tunnel so that issues such as wall effects could be eliminated. For large jet momentum flux ratios, tests conducted in the external flowfield surrounding a supersonic aircraft become attractive from an economic viewpoint. From a technical viewpoint, such an aircraft would provide a realistic and reliable test environment over all Mach numbers of interest, including the Mach 1.0 region.

Through the cooperative efforts of personnel at UCLA and the NASA Dryden Flight Research Center, an agreement was made by which researchers at UCLA would be able to use Dryden's F-104G research aircraft #826 as a "flying wind tunnel" platform for the transverse jet experiments; Figure 1.4. During the 1960's, the Lockheed F-104G was modified to carry a low aspect ratio fin on the underside of the fuselage for the purpose of conducting panel flutter tests in a flight environment. This "flight test fixture" (FTF), as it is known, has evolved into a highly versatile facility for aerodynamics and fluid mechanics research [Meyer (1982)]; Figure 1.5. The capabilities of the FTF include (1) a large Mach number envelope (0.4 to 2.0), including the region through Mach 1.0 with no adverse effects, (2) the ability to test articles or study flowfields larger than those that can accurately be tested in wind tunnels, (3) a larger Reynolds number and dynamic pressure envelope than most tunnels. In addition, a flight trajectory guidance system uplinks engineering parameters calculated on a ground-based computer (using aircraft and/or FTF telemetry) to the cockpit display so the pilot can maintain desired flight test conditions. The result is that some unique trajectories are routinely flown, including constant Reynolds number profiles, dynamic pressure versus Mach number profiles, and constant Mach number, altitude, and angle-of-attack profiles. Over the years, the flow environment around the FTF has been well-characterized through the use of a variety of pressure and boundary-layer measurement techniques. The F-104/FTF testbed suits our needs very well in terms of achieving a wide range of Mach numbers at various pressures/altitudes so that a perfectly expanded gas jet can be formed.

As illustrated in Figure 1.6, the jet will originate from the side of the FTF and turn in to the crossflow. A nitrogen jet seeded with iodine was chosen to be the injectant. As far as simulating the actual fuel-injection process of hydrogen (lighter than nitrogen) into air, previous work has suggested that fuel penetration and spreading are insensitive to fuel molecular weight [McDaniel and Graves (1988)]—so that nitrogen is an acceptable choice. Keep in mind, however, that the injectant and air are nonreacting. The trajectory, spreading, and mixing of the jet are determined by illuminating a horizontal cross-section of the nitrogen jet with a sheet of light from a Nd:YAG laser, the fluorescence resulting from the iodine seed excitation. This method of flow visualization is known as planar laser-induced fluorescence or "PLIF" and is discussed in greater detail in section I.3. The flowfield images are captured by a high-speed gated intensified video camera synchronized to the laser pulse rate and equipped with appropriate optical filters to improve the signal-to-noise—the noise being wavelengths outside the iodine fluorescence spectrum. All components needed to generate, seed, and control the jet are housed inside the FTF in
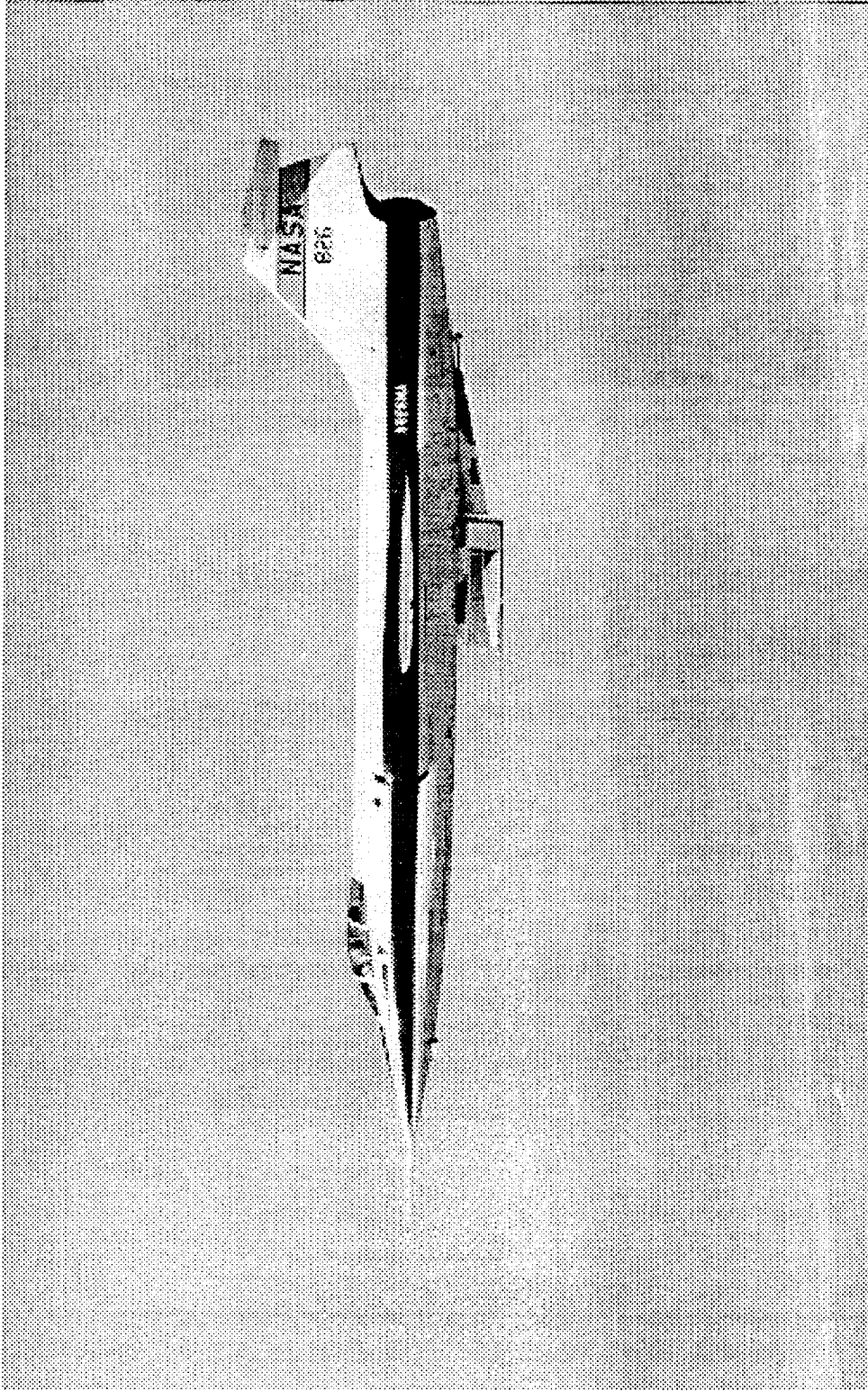
Figure 1.4 Photo of F-104G with Flight Test Fixture
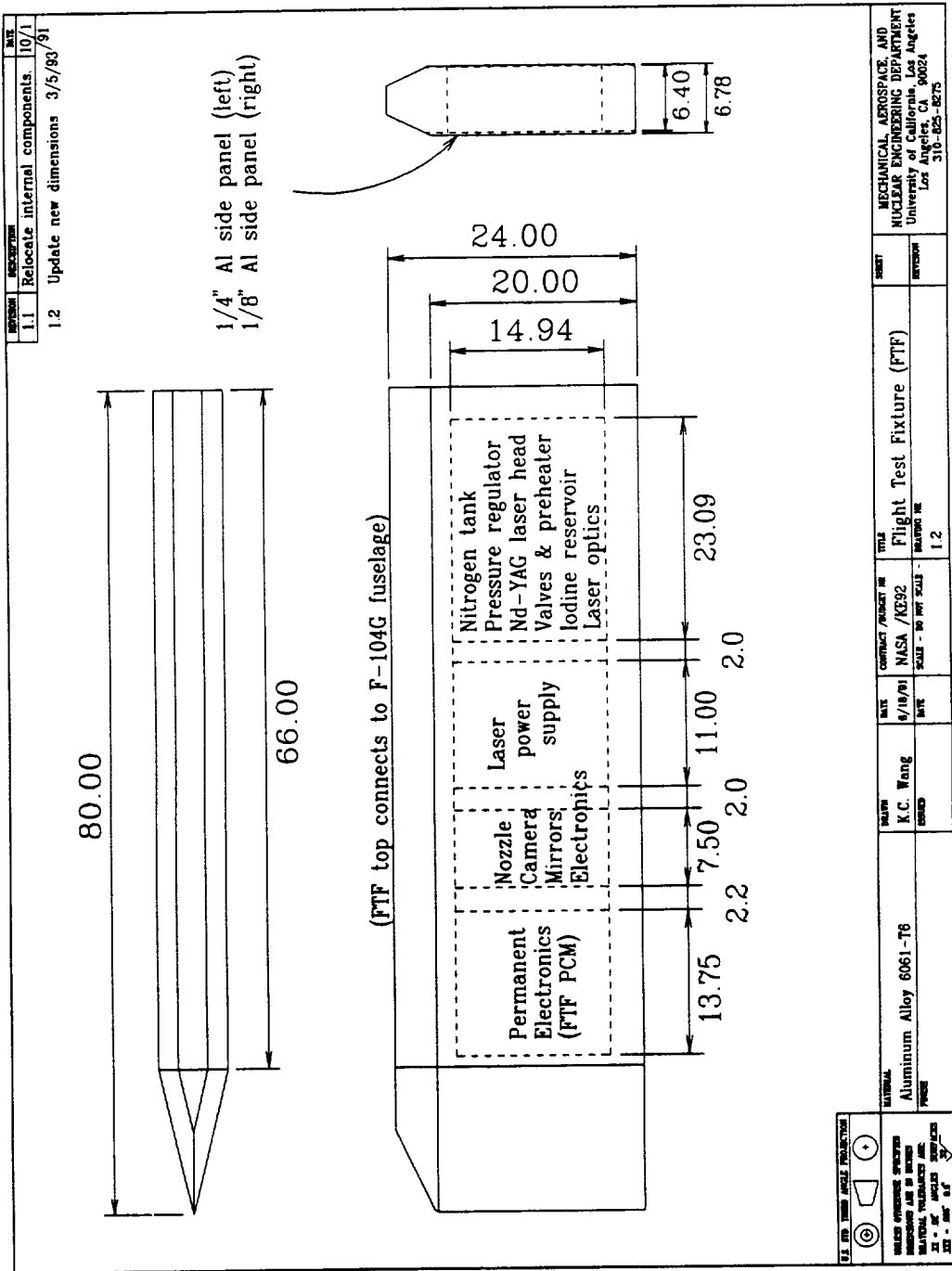
Figure 1.5 Schematic of Flight Test Fixture
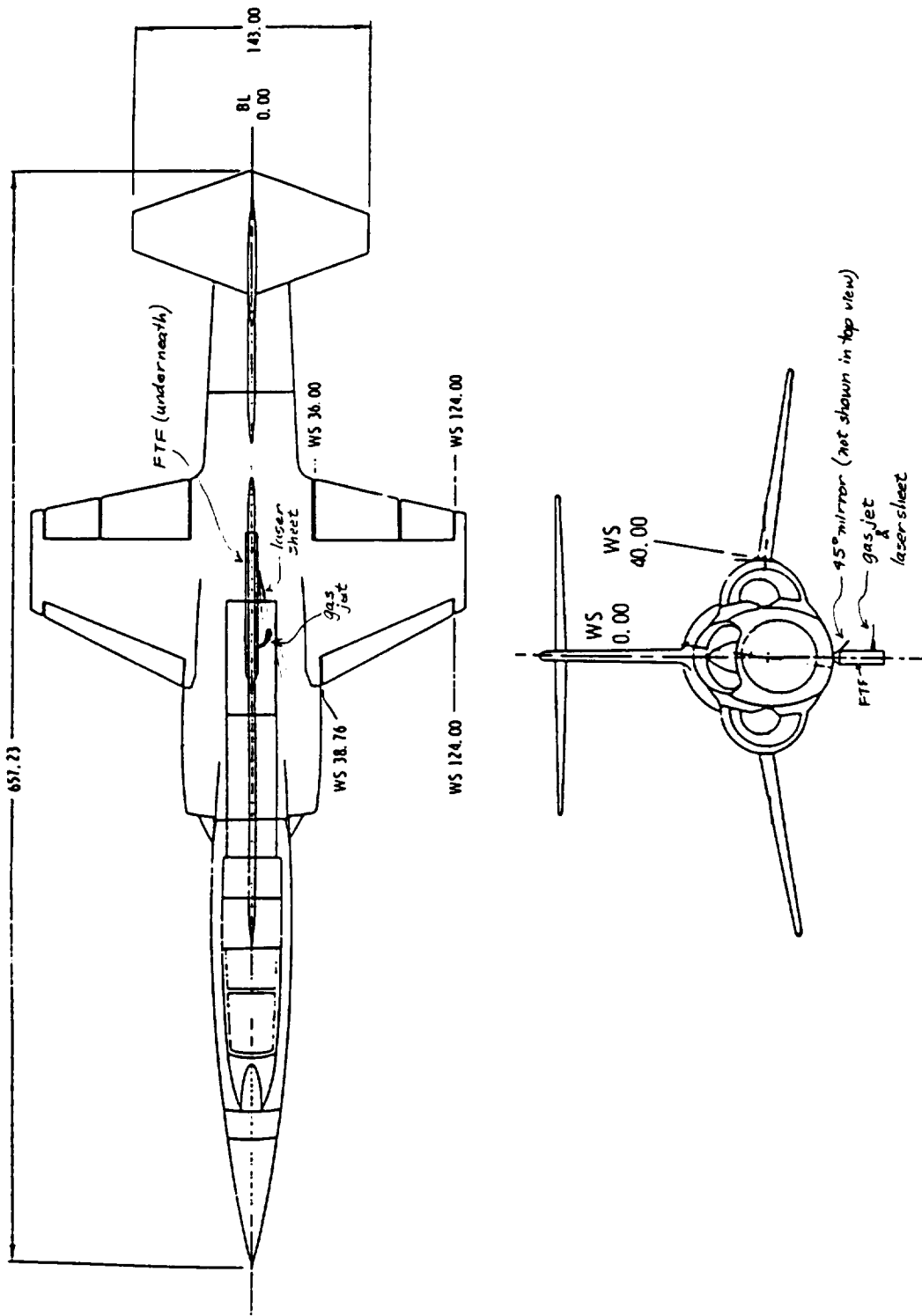
Figure 1.6 Schematic of F-104G with Flight Test Fixture

11

an internal components rack called the ICR. No external modifications to the FTF or aircraft are made. The laser, video camera, and associated electronics are also assembled inside the ICR. The complete assembly can be categorized into three subsystems: the illumination subsystem, the image acquisition subsystem, and the jet formation subsystem. These are detailed individually and collectively in sections II.1 through II.4.

I.3 Theoretical Considerations

Theoretical considerations were given to (1) the method of flow visualization, (2) the means of image acquisition, and (3) the mathematical aspects of the experiment's thermodynamics and fluid mechanics.

I.3.1 The Method of Flow Visualization

Planar laser-induced fluorescence (PLIF) is a nonintrusive method of flow visualization applied to gaseous as well as liquid flows [Merzkirch (1987)]. For gaseous flows, visualization is achieved by seeding the primary gas flow with a gaseous fluorescent tracer, whose molecules emit a characteristic fluorescent radiation upon excitation by light of an appropriate wavelength. When a seeded flowfield is excited by a laser beam or planar sheet, the tracer molecules are pumped to a higher electronic energy level, from which they spontaneously decay to an intermediate energy level, so that the emitted radiation is of a wavelength different from that of the exciting light. An appropriate narrow optical filter, such as a band-pass or interference type, allows for blocking off noise generated by the incident as well as background light.

The fluorescence signal is a function of the pressure, temperature, density, and chemical composition of the flow, and complex equations exist to analyze these physical parameters [Lee et al. (1992)], leading to quantitative deductions of the flow properties. Our present scope, however, is more quantitative. From a first-order analysis, it follows that the intensity of the emitted fluorescence is proportional to the number density of the tracer molecules in the scattering volume. Since one generally assumes that the tracer molecules are uniformly distributed in the flowing gas, one concludes from the recorded light intensity onto the local value of the gas density in the compressible flow. Details of our particular PLIF setup are given in section II.1.

I.3.2 The Means of Image Acquisition

Electronic imaging of the flowfield is provided by a gated intensified camera. The core of the intensified camera is the electronic imaging tube, whose basic parts are shown in Figure 1.7 [from Csorba (1990)]. Image intensifier tubes are used to intensify faint images and make them bright and perceivable to the human eye. The light image (target) to be amplified is first focused on a photocathode by the camera's lens. Upon absorption, the incident radiant energy is converted to photoelectrons, forming a low energy input photoelectron image on the photocathode. These photoelectrons are then accelerated by a high voltage power supply toward a microchannel plate (MCP). The current-multiplying MCP multiplies the electrons in cascade fashion. The number of electrons that is generated in this manner depends on the voltage applied between the two sides of the MCP. After

12

Labels in figure:
- Target
- Objective lens
- Image of the target
- Glass or fiberoptic faceplate
- Conductive coating
- Phosphor screen
- Ceramic metal body
- Intensified image
- Laser beam
- -1000 V
- -800 V
- Microchannel plate
- Photocathode
- +6 kV
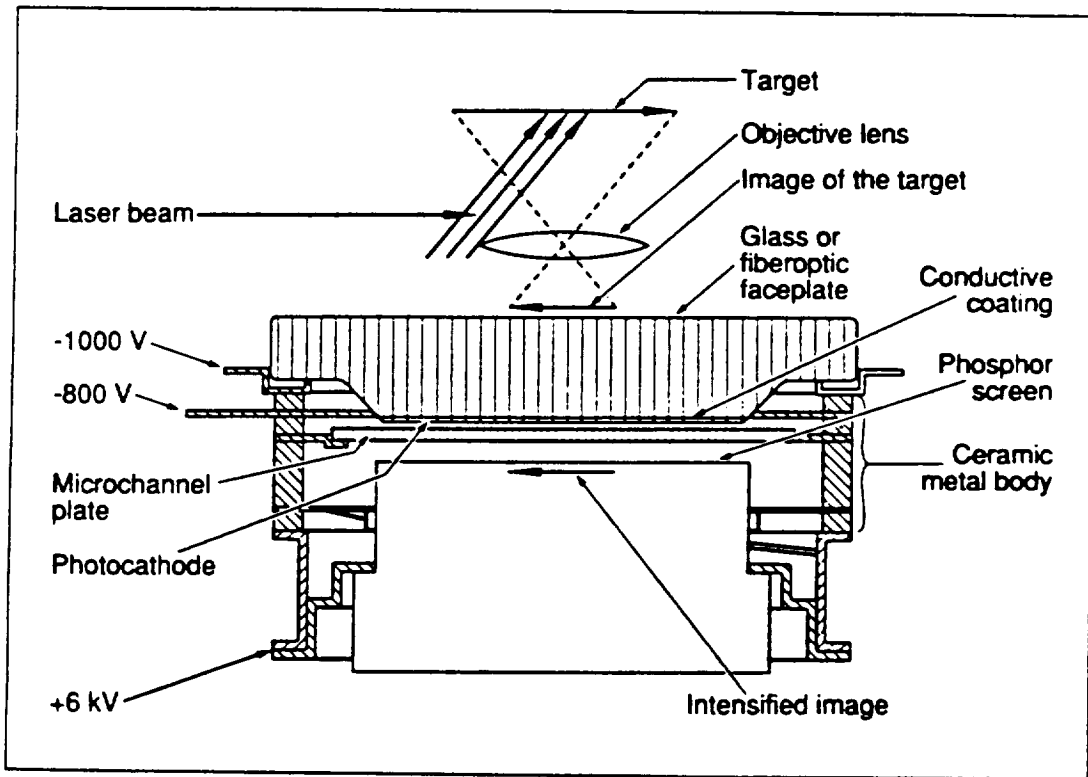
Gated intensifiers synchronize image acquisition with laser pulses to improve visibility and record transient events.

Figure 1.7 Basic Parts of an Image Intensifier [Csorba 1990]

exiting the MCP, the photoelectron image is accelerated by an applied voltage toward a fluorescent phosphor screen. There the kinetic energy of the photoelectrons is converted into an intensified light image, which is transmitted through a fiber optic bundle to a CCD array for further image processing before terminating in a video monitor. Images 10,000–100,000 times brighter are made possible with intensified camera imagery. Use of the MCP is characteristic of "Generation II" intensifier tubes [Csorba (1988)]. Our current application also involves gating circuitry allowing the intensifier to be gated "on" in synchronization with the pulses of the illuminating laser. This further increases the signal-to-noise by selectively "blocking out" image frames where no illumination (and thus no fluorescence) is taking place.

I.3.3 Mathematical Aspects

The mathematical aspects of the experiment focused on two primary areas of analytical and design interest: (1) on understanding the flowfield across the FTF at various altitudes and free-stream velocities, and (2) on predicting the thermodynamics and power requirements to form the transverse gas jet. Two FORTRAN programs, included in the Appendix, were created to address these preliminary design issues.

The first code, FTF1, determines the pressure, density, and temperature just outside the jet exit orifice for all altitudes from 2,500 to 50,000 ft based on aircraft Mach number and the angle of the oblique shock, β, off the tip of the FTF. We assume a standard atmosphere, ignoring seasonal changes, as defined by the *U.S. Standard Atmosphere, 1976* handbook. This approximation is valid for altitudes above 15,000 ft, and is acceptable for our needs since we do not conduct any experiments below this altitude. To obtain a perfectly expanded gaseous jet, the free-stream pressure outside the orifice (∞), also known as the back pressure, must equal the jet pressure at the nozzle exit.

$$P_\infty = P_{jet} \tag{1.2}$$

This is achieved by having the pilot fly to an altitude where the free-stream back pressure is known to match the jet exit pressure for the given free-stream Mach number. But since the jet exit pressure is inherently fixed (cannot be adjusted in flight) and several Mach numbers must be tested (0.8–2.0), the pilot must fly at different altitudes for different Mach numbers to provide the appropriate back pressure. It is not critical that equation (1.2) be exactly met. Though we are particularly interested in the perfectly expanded jet, overexpanded jets are acceptable as well, as far as validating the numerical correlations of Heister and Karagozian (1990ab) is concerned.

The basis for choosing the target jet exit pressure was twofold, both dealing with temperature. On one hand, the ambient temperature at the jet exit should be as high as possible to ensure the iodine vapor fluoresces and does not condense—suggesting low altitudes and thus a higher fixed/atmospheric pressure. On the other hand, the ambient temperature must not exceed the maximum inlet air temperature limit of the F-104's engines—suggesting high altitudes and a lower fixed/atmospheric pressure. At the advice

of NASA personnel familiar with the F-104, we were told that 40,000 ft at Mach 2.0 flight would be ideal for the aircraft.

Using the FTF1 code, this altitude/speed combination produces a free-stream pressure outside the jet orifice of 39,000 Pa, or about 0.38 atm. The jet formation subsystem was adjusted (via a pressure regulator) to provide the necessary 39 kPa at the jet exit. With the "target pressure" selected, the FTF1 code was run for the different Mach numbers below 2.0 to determine which altitudes corresponded to the same target pressure. Results are shown in Figure 1.8. Note: the altitudes for Mach numbers 0.8–1.4 were interpolated to a first approximation since the shock off the tip of the FTF at these speeds is detached and no reliable analytical formulation exists to solve for it.

The numerical code provides the desired free-stream conditions by calculating the flow properties in four separate flow regions, as shown in Figure 1.9. Region 1 is the flow far ahead of the aircraft. Upon reaching the FTF, the air flow crosses an oblique shock produced by the 25.75° wedge tip of the FTF, and is turned laterally into region 2. We assume adiabatic flow of a calorically perfect gas, so the appropriate relations are:

$$M_{n_1} = M_1 \sin\beta \tag{1.3}$$

$$\frac{\rho_2}{\rho_1} = \frac{(\gamma+1)\,M_{n_1}^2}{(\gamma-1)\,M_{n_1}^2 + 2} \tag{1.4}$$

$$\frac{p_2}{p_1} = 1 + \frac{2\gamma}{\gamma+1}\,(M_{n_1}^2 - 1) \tag{1.5}$$

$$M_{n_2}^2 = \frac{M_{n_1}^2 + [2/(\gamma-1)]}{[2\gamma/(\gamma-1)]\,M_{n_1}^2 - 1} \tag{1.6}$$

$$\frac{T_2}{T_1} = \frac{p_2}{p_1}\frac{\rho_1}{\rho_2} \tag{1.7}$$

$$M_2 = \frac{M_{n_2}}{\sin(\beta-\theta)} \tag{1.8}$$

15

FLIGHT ENVELOPE

NO EXTERNAL STORES EXCEPT AS NOTED
GROSS WEIGHT - 16000 LB.
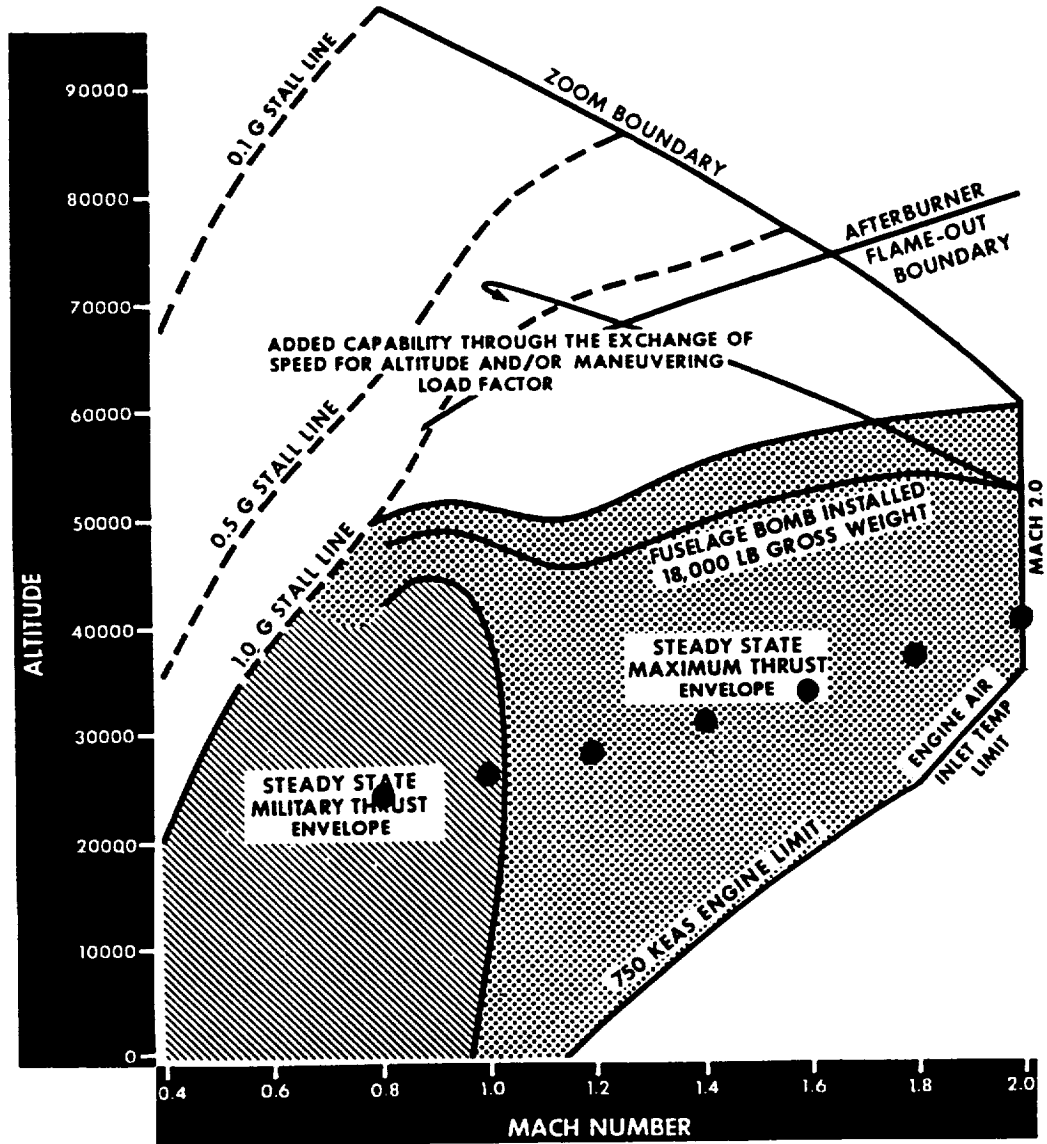
Figure 1.8 F-104G Flight Envelope and Target Conditions

Oblique shock

Expansion fan

Freestream flow

Bow shock

① ② ③ ④

Transverse jet

View of FTF looking down on transverse jet.
Note the four distinct regions of flow.
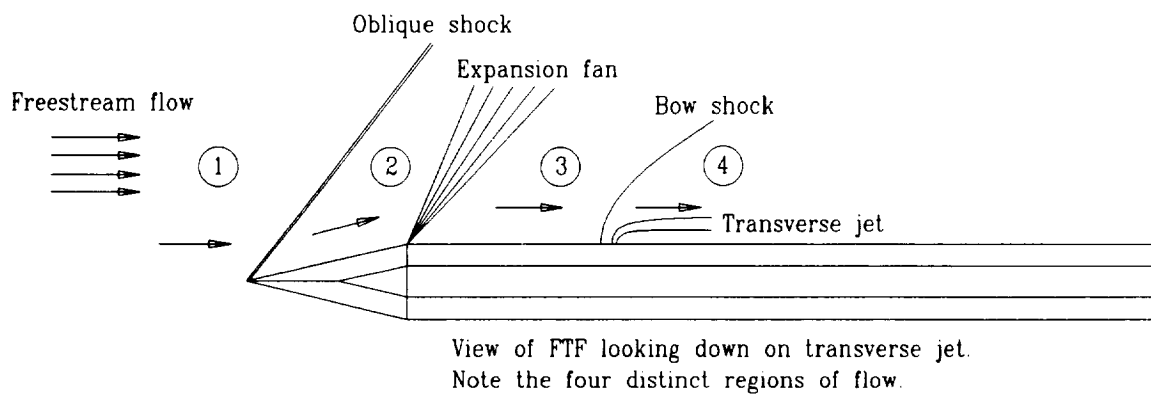
Figure 1.9   FTF1 Schematic of Analysis

17

Theta, the deflection angle, is simply half the wedge angle and equals 12.875°. Beta, the oblique shock angle, can be deduced from a plot of the following equation, known as the $\theta - \beta - M$ relation:

$$\tan\theta = 2\cot\beta \left[\frac{M_1^2 \sin^2\beta - 1}{M_1^2 (\gamma + \cos 2\beta) + 2} \right] \qquad (1.9)$$

Such a plot may be found in any text on compressible fluid mechanics; for example, Anderson (1990).

Upon reaching the shoulder of the FTF, the flow of region 2 is expanded isentropically through a Prandtl-Meyer expansion fan/wave into region 3. The properties are calculated using the relation:

$$\theta_3 = \nu(M_3) - \nu(M_2) \qquad (1.10)$$

where $\nu(M)$ is known as the Prandtl-Meyer function:

$$\nu(M) = \sqrt{\frac{\gamma+1}{\gamma-1}} \tan^{-1} \sqrt{\frac{\gamma-1}{\gamma+1}(M^2 - 1)} - \tan^{-1}\sqrt{M^2 - 1} \qquad (1.11)$$

Equations 1.10 and 1.11 are solved numerically in FTF1 using the secant method. The obtained result is M_3. Because the flow is isentropic, T_0 and p_0 are constant through the wave, so that T_3, p_3, and ρ_3 only depend on M_3:

$$T_3 = T_2 \frac{1 + \frac{\gamma-1}{2}M_2^2}{1 + \frac{\gamma-1}{2}M_1^2} \qquad (1.12)$$

$$p_3 = p_2 \frac{T_3}{T_2}^{\frac{\gamma}{(\gamma-1)}} \qquad (1.13)$$

$$\rho_3 = \rho_2 \frac{T_3}{T_2}^{\frac{1}{(\gamma-1)}} \qquad (1.14)$$

Lastly, the flow encounters a bow shock just ahead of the gas jet. The properties of region 4, behind the bow shock, are found using the following numerically-derived correlations by Heister and Karagozian (1990a).

$$p_4 = p_3 (0.405 + 0.426 \ M_3^2) \qquad (M_3 \geq 1.5)$$

$$= p_3 (0.861 + 0.217 \ M_3^2) \qquad (0.8 < M_3 < 1.5)$$

$$= p_3 \qquad (M_3 \leq 0.8) \qquad (1.15)$$

$$\rho_4 = \rho_3 [0.651 + 0.805 \ ln \ (M_3)] \qquad (M_3 \geq 2.0)$$

$$= \rho_3 (0.964 + 0.0565 M_3^2) \qquad (0.8 < M_3 < 2.0)$$

$$= \rho_3 \qquad (M_3 \leq 0.8) \qquad (1.16)$$

The temperature is approximated through the ideal gas law:

$$T_4 = \frac{p_4}{\rho_4 R} \qquad (1.17)$$

For purposes of finding the crossflow Mach number at the jet exit, M_4, the bow shock can be approximated as a normal shock:

$$M_4 = \sqrt{\frac{1 + [(\gamma - 1)/2] M_3^2}{\gamma M_3^2 - (\gamma - 1)/2}} \qquad (1.18)$$

In summary, the user inputs a particular free-stream M_1 and corresponding shock angle, β, based on M_1 and the deflection angle of the FTF wedge tip, θ. The code then gives the pressure, density, temperature, and velocity of the flow at the jet exit for all altitudes up to 50,000 ft in intervals of 2,500 ft. The user then selects the altitude at which p_4 equals the target pressure of 39 kPa for a perfectly expanded jet. If the pressure values are slightly different, the user is asked to choose the altitude that provides a slightly underexpanded jet, i.e., the higher altitude. The code provides a theoretical estimate of the flow properties at all regions of interest and in turn dictates the flight plan needed for the experiments, in terms of altitude and Mach number (Figure 1.8).

The second code, FTF2, determines the thermodynamic conditions along the flow through the jet formation subsystem. It also gives the power requirements for necessary gas heating. We approach the analysis by working backward from the nozzle to the nitrogen and iodine tanks. We know $p_4 = p_{exit} = 39$ kPa. We additionally require T_{exit} to be above 373 K. The temperature must remain high in order that the iodine does not condense prior to exiting or soon thereafter. Also, it increases the population of the high ($50 < j < 100$) rotational states of iodine that are accessible at 532 nm for fluorescence. In practice, this value will vary somewhat depending on how long a particular test is run, due to the heating transients. The analysis of FTF2 assumes quasi one-dimensional flow of an ideal gas.

Following the nomenclature of Figure 1.10, we calculate the pressure and temperature of the nitrogen/iodine mixture in section 6 in the following manner, taking advantage of the constant stagnation properties. The nozzle area ratio is 2:1, so that if $M_{exit} = 1.0$, then $M_6 = 0.306$.

$$p_6 = (1 + \frac{\gamma-1}{2}M_6^2)^{-\frac{\gamma}{\gamma-1}}(1 + \frac{\gamma-1}{2}M_{exit}^2)^{\frac{\gamma}{\gamma-1}}p_{exit} \tag{1.19}$$

$$T_6 = (1 + \frac{\gamma-1}{2}M_6^2)^{-1}(1 + \frac{\gamma-1}{2}M_{exit}^2)T_{exit} \tag{1.20}$$

The pressure p_6 is maintained during experiments by a pressure regulator on the nitrogen tank, and monitored by pressure transducers located at sections 0, 1, and 6. The temperature T_6 is achieved through the use of heating tapes around the gas lines and a nitrogen preheater, all monitored by digital temperature controllers. The preheater is necessary to counteract the Joule-Thompson cooling effect across the regulator as well as to heat the nitrogen high enough prior to iodine seeding to prevent iodine condensation.

Power requirements for the preheater are calculated from the simple relation:

$$q = \dot{m}c_p(T_2 - T_1) \tag{1.21}$$

where $\dot{m}$, which is approximately constant between sections 1 and the exit, is calculated as:

$$\dot{m} = \rho_{exit}v_{exit}A_{exit} \tag{1.22}$$

Volumetric flow rate is deduced by dividing $\dot{m}$ by density. The mass flow rate of iodine is selected to provide a 2000 ppm seeding of iodine vapor into the nitrogen mass flow. The orifice of the iodine valve is 0.116 in. and a pressure differential of about 2:1 across the valve is chosen to facilitate proper seeding/flow. Iodine pressure is controlled by maintaining high enough temperatures in the iodine reservoir. According to the vapor pressure versus temperature chart in Hultgren et al. (1973), a temperature of 458 K (185 °C) will provide an iodine vapor pressure of 101 kPa (1.0 atm). And according to the CRC Handbook of Chemistry and Physics, 190 °C will provide 1.10 atm, 195 °C will provide 1.22 atm, and 200 °C will provide 1.37 atm. The 200 °C/1.37 atm setting corresponds exactly to a 2:1 pressure differential, although any of the above temperatures should deliver adequate iodine concentrations for fluorescence.

Nitrogen supply requirements are also computed by FTF2. The nitrogen tank holds 5.1 liters, and typical pressures will go up to 3000 psi. Knowing the amount of nitrogen in the tank and the mass flow rate, we find that we can support more than ten 10-second test runs, without experiencing appreciable stagnation pressure loss due to nitrogen depletion. Iodine supply requirements are similarly calculated. Typically, we supply at least 10 grams of iodine per nitrogen refill.
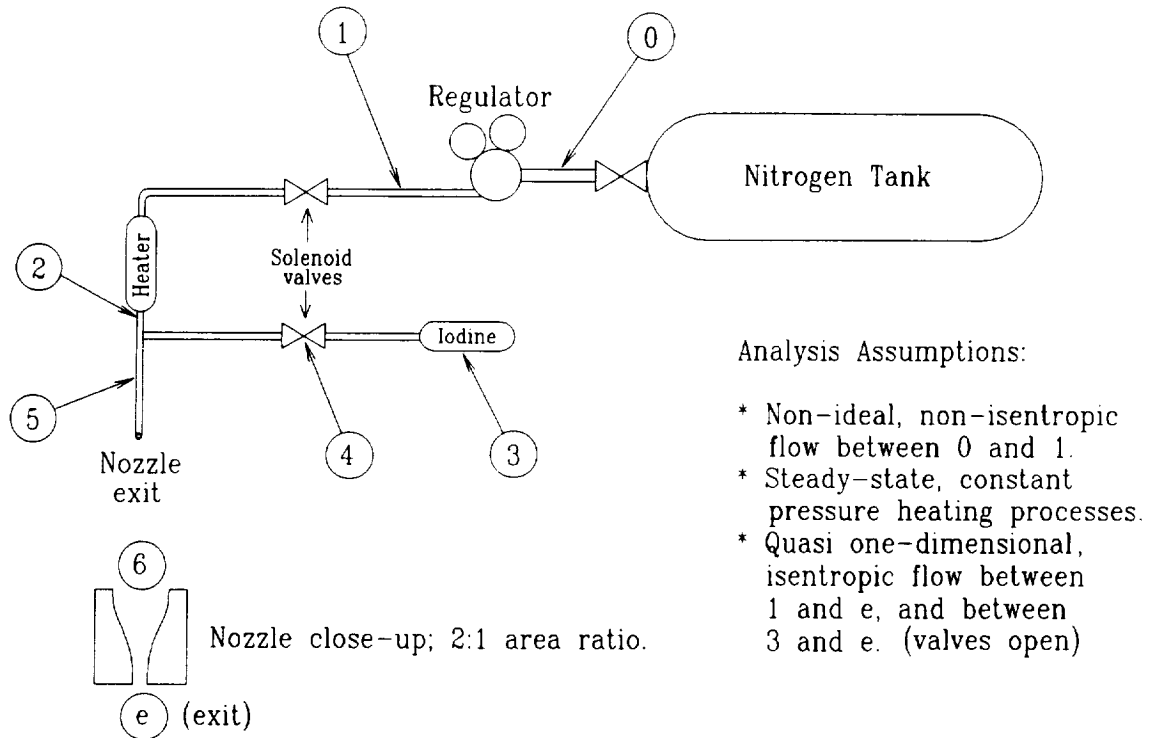
Figure 1.10   FTF2 Schematic of Analysis

CHAPTER II
EXPERIMENTAL SETUP

The experimental apparatus can be categorically divided into three associated subsystems. The illumination subsystem consists of the laser and its associated optics. The image acquisition subsystem is comprised of the intensified camera and its filters and mirrors responsible for imaging the fluorescent jet. The jet formation subsystem includes all components involved in the storage, pressure regulation, heating, and flow control of the nitrogen gas and iodine seed. The three distinct subsystems are mechanically integrated using a unique internal components rack (ICR) and remotely controlled through analog and digital electronics, also mounted on board the ICR.

II.1 The Illumination Subsystem

We use the 2nd harmonic of a Nd:YAG laser at 532.25 nm to pump several lines in the R and P branches of the B ← X transition for I_2; the R(56) (32-0) line at 18788.348 cm^{-1}, the P(83) (33-0) and R(134) (36-0) lines around 18787.814 cm^{-1}, and the P(53) (32-0), P(103) (34-0) and P(159) (39-0) lines around 18788.453 cm^{-1}. A Q-switched (pulsed) diode pumped laser (Adlas DPY 321 QD) is used, operating in the broadband mode with visible green/yellow light. Its specifications are given in Figure 2.1. Operating in this mode, the laser linewidth is approximately one wavenumber, so that none of the lines listed above are individually resolved; rather, all the lines are simultaneously excited.

The I_2 B ← X system has been used successfully in this application by McDaniel and Graves (1988) and Fletcher and McDaniel (1990). In these wind tunnel experiments, an argon ion CW laser (which pumps different ro-vibronic states) was used. In an aircraft borne experiment, the Nd:YAG laser selected has several important advantages in comparison to the argon ion laser.

- cavity dumped laser such as the Nd:YAG is much less sensitive to alignment problems caused by vibration and temperature variations than a high-gain CW laser. The laser selected for our experiments has been used successfully aboard transport aircraft [Sitz and Farrow (1990), Simmons and Hougen (1977)].

- The Adlas laser has a very low power consumption (< 50 W; typ. 30 W), needs no external cooling and utilizes only low voltages internally.

- Because the Nd:YAG is pulsed, for a given electrical load the peak power is much greater, in our case greater than 1.6 kW. If advantage is taken of lightweight, robust gated cameras, it is possible to obtain considerably better signal-to-noise ratio at a given electrical load, or equivalently to obtain about the same signal-to-noise at a much reduced load.

- The Adlas laser is very compact and light weight. (Head: 14.3 × 3.5 × 3.5; PS: 15 × 5.1 × 10.2 in.; combined weight: 29 lb)

22

Specifications

diode laser pumped solid state lasers, q-switched
1064 / 1047 / 532 / 523 nm

(Nd:YAG)
Nd:YLF

Technical Data	101Q	201Q	301Q	321Q	101QD	201QD	301QD	(321QD)
wavelength (nm)	1064				532			
	1047				523			
max.pulsed peak power (kW)	>0.12	>0.6	>2.7	>5	>0.03	>0.13	>0.8	>1 6
	>0.25	>1.2	>5.3	>9	>0.06	>0.3	>1.6	>2.8
shortest possible pulse length (ns)	<40	<25	<15	<15	<35	<23	<13	<13
max.pulse energy (µJ)	>5	>15	>40	>75	>1	>3	>10	>20
	>10	>30	>80	>130	>2	>7	>20	>35
repetition rate (Hz)	0-1000 full pulse specs./>1000 reduced pulse specs.							
	0-500 full pulse specs./>500 reduced pulse specs.							
TEM$_{00}$ beam diameter, typical (mm) (I/e^2)	0.9				0.35			
TEM$_{00}$ beam divergence (mrad) (I/e^2)	2.0				2.0			
beam pointing stability (% of beam divergence)	<±10				<±10			
pulse to pulse stability (%)	s = 2%				s = 5%			
stability of average output power over 2 hours (%)	typ ±1%				typ ±2%			
polarization	linear 100:1							
operating voltage	110/220V AC ±10%							
power consumption	<50W (typ. 30 W)							
input signal for external control	TTL							
ambient temperature range for operation	0-30° C (32-85° F)							
dimensions of laser head (mm/inches)	230x72x57 9.1x2 8x2.2		236x90x80 9.3x3.6x3.2	370x88x88 14x3.5x3.5	230x72x57 9.1x2 8x2.2		236x90x80 9.3x3 6x3.2	370x88x88 14x3.5x3.5
dimensions of power supply (mm/inches),weight	230x107x150 3.5 kg 9.1x4.2x5.9 7.7 lbs			380x130x260 9 kg 15x5.1x10.2 20 lbs	230x107x150 3.5 kg 9.1x4 2x5.9 7 7 lbs			380x130x260 9 kg 15x5.1x10.2 20 lbs
weight of laser head g	800	1500	3400		800	1500	3400	
oz	28	53	136		28	53	136	

Design and technical data are subject to change without notice

Replacing tubes by semiconductors

| DANGER | DANGER |

⊁ADLAS
advanced design lasers

Figure 2.1 Adlas DPY 321 QD Specifications

23

This reduced power consumption is very important in the present application. Not only is power limited, but rejection of waste heat can also be a problem. Cooling requirements for our laser head and power supply are relatively low, making it possible to reject heat to the ambient air via natural convection. As an added measure, the laser head is equipped with a thermocouple feedback and internal fan in case forced convection is needed. The use of low voltages is also important, since the experiment is operated in pressure ranges where arcing occurs most easily. The laser manufacturers have specially modified the laser power supply to run from the 28 VDC power aboard the F-104G aircraft.

A further potentially useful feature of the Nd:YAG is the possibility of single-mode (injection seeded) operation, reducing the linewidth to 0.0045 wavenumbers. The added ability to scan over about one wavenumber allows not only the resolution of individual lines, but also the determination of lineshapes. This is illustrated in Figure 2.2, which depicts fluorescence obtained by scanning the pump laser over several fully resolved lines in the I_2 spectrum around 532 nm. The above result was obtained using an injection seeded Nd:YAG laser and an iodine cell at a number density of 10^{16} molec/cm^3 [Sitz and Farrow (1990)]. Peak assignments are derived from Simmons and Hougen (1977). Fluorescence intensity using the same laser in the multimode configuration is shown for comparison. Higher peak signals for single-mode operation are a result of the higher spectral energy density of the injection seeded laser.

If injection seeding can be made to work aboard the aircraft, this would allow us to image the jet temperature and the velocity component in the direction of beam propagation. The velocity component can be derived from the Doppler shift of the line centers. Jet temperature can be derived from the lineshape.

Effective iodine seed concentrations were determined in preliminary tests using a custom-built "iodine reference cell," built by the UCLA Department of Chemistry Glass Shop. The cell allows iodine vapor to be confined at a specified number density. Tests with number densities similar to what is expected in the jet have shown that we can easily achieve fluorescence intensities large enough to see against a background of normal room light, provided that the intensified camera is gated to the laser pulse rate. The same tests conducted in moderate outdoor sunlight show that fluorescence can be observed above the background, although the signal-to-noise ratio is not nearly as good as for the indoor tests. These tests utilized a long pass Shott glass filter with a cut-on wavelength of 550 nm. Analysis of the fluorescence spectrum from 540–610 nm (Figure 2.3) shows the filter is attenuating 80–90 percent of the strongest fluorescence band (between 540–545 nm). We expect to improve the signal-to-noise in daylight environments by using more appropriate band-pass or interference filters centered around 532 or 542 nm.

The laser and sheet formation optics are housed within the ICR as shown in Figures 2.4 and 2.5. The sheet is formed by means of a –6.35-mm focal length front surface cylindrical mirror (1) that expands the beam horizontally. A high-reflectivity mirror (2) housed in the optical canopy (3) acts as a turning mirror, positioning the light sheet on the jet plane. This positioning is dependent on the angle of attack (+3° alpha in level flight), so provision or adjustment is made via a multi-axis kinematic mirror mount. This mirror mount also serves to orient the edge of the laser sheet parallel to the flight test fixture and

Fluorescence Excitation
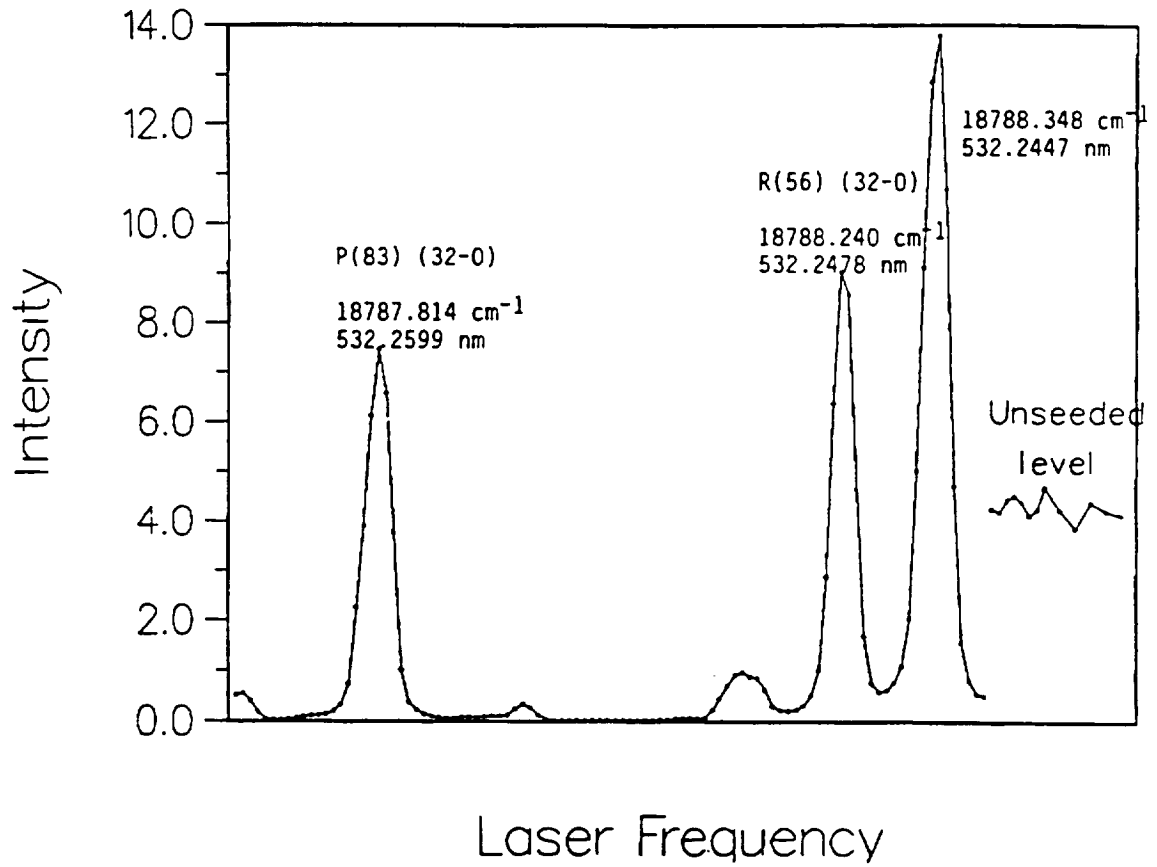
Fluorescence of iodine lines around 532 nm. This spectrum was obtained at Sandia National Laboratories with an single mode (injection seeded) Nd:Yg laser. Fluorescence intensity from broadband excitation of the same lines is shown for comparison.

Figure 2.2 Iodine Fluorescence Excitation
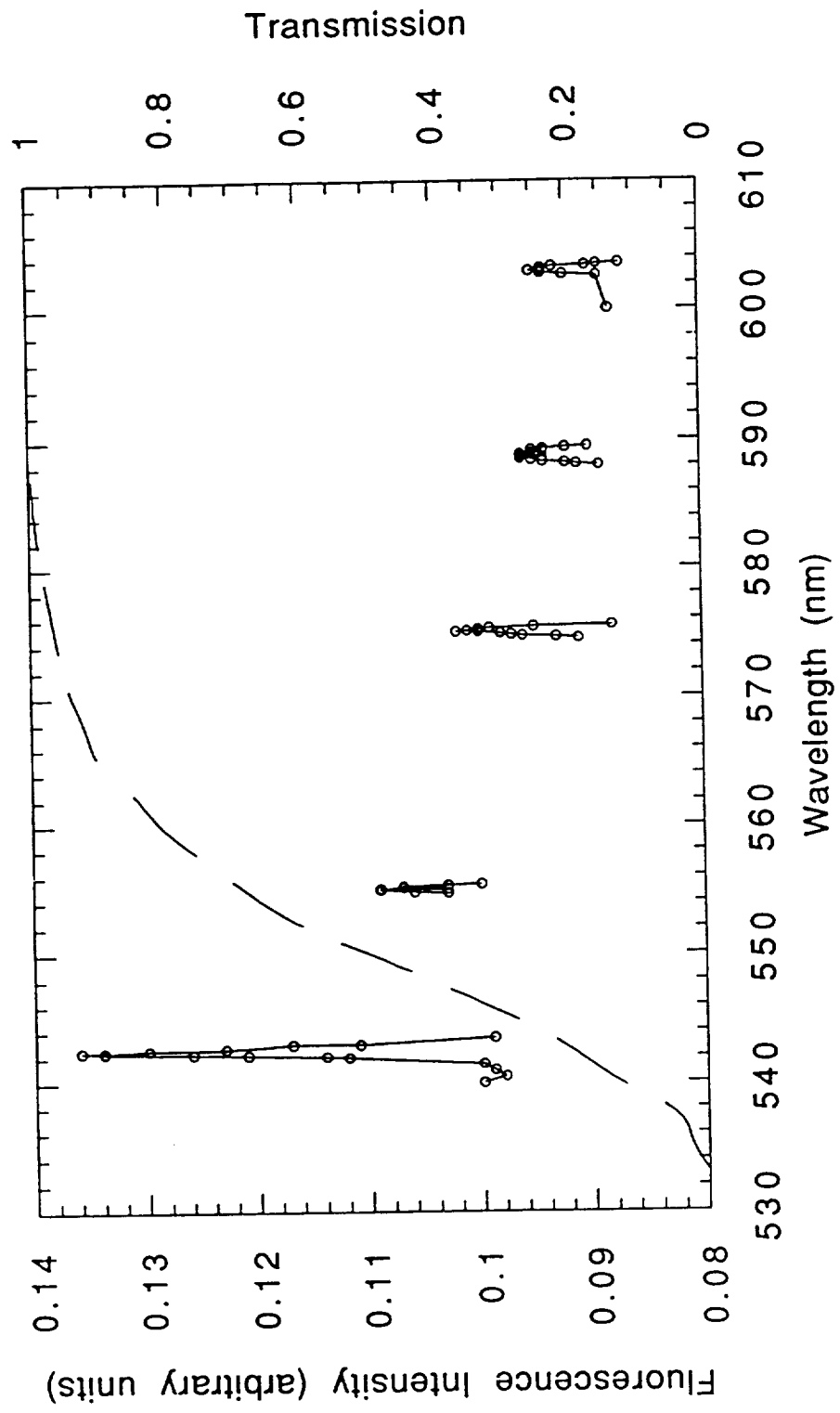
Figure 2.3   Iodine fluorescence spectrum between 540-610 nm.
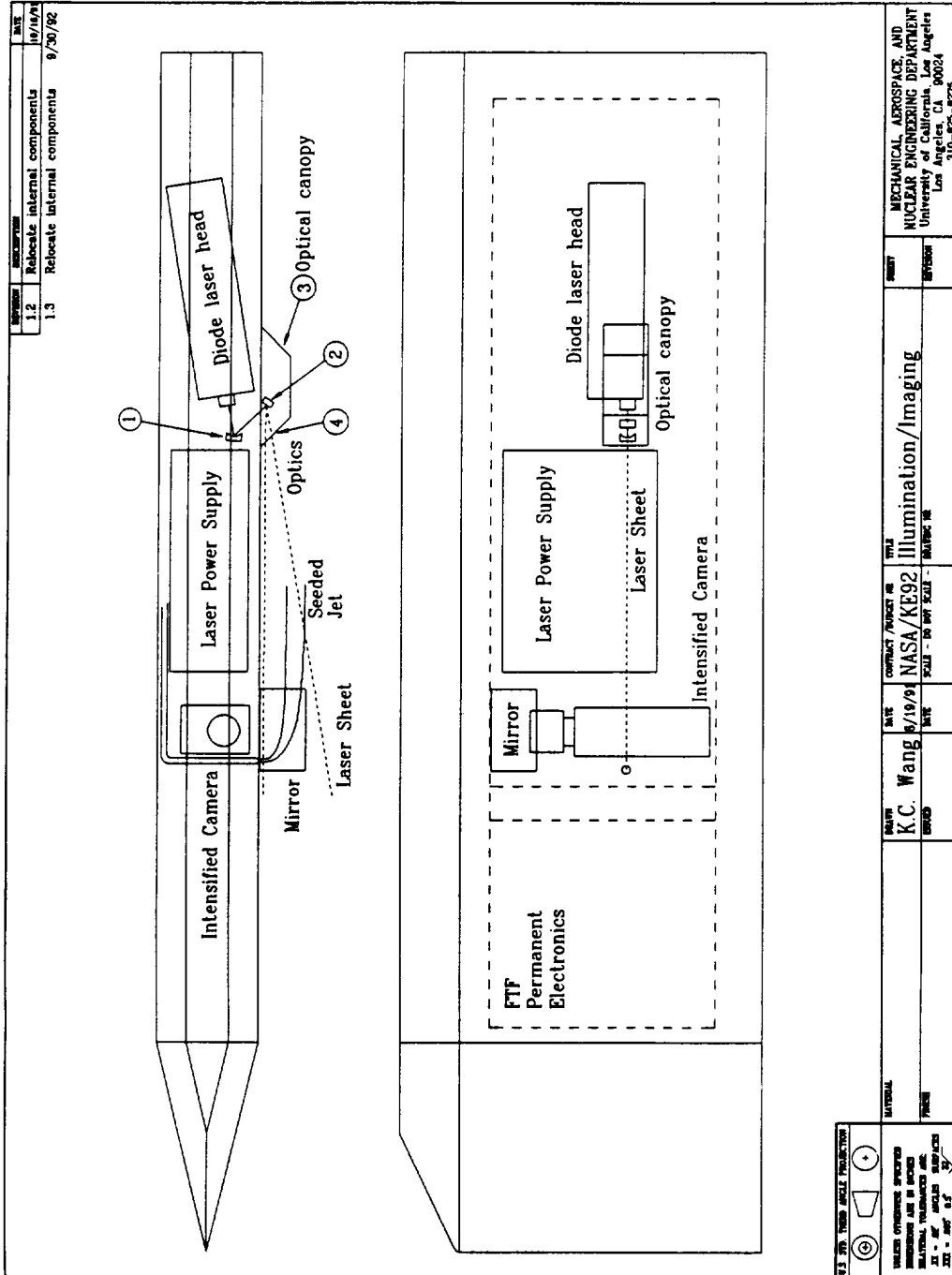
Figure 2.4   Schematic of Illumination and Image Acquisition Subsystems

REVISION	DESCRIPTION	DATE
1.2	Relocate internal components	10/16/91
1.3	Relocate internal components	9/30/92

Diode laser head

③ Optical canopy

②

①

④

Optics

Laser Power Supply

Seeded Jet

Intensified Camera

Mirror

Laser Sheet

Diode laser head

Optical canopy

Laser Power Supply

Laser Sheet

Intensified Camera

Mirror

o

FTF Permanent Electronics

DRAWN	DATE	CONTRACT/PROJECT NR	TITLE
K.C. Wang	5/19/91	NASA/KE92	Illumination/Imaging

SCALE - DO NOT SCALE -

SHEET   MECHANICAL, AEROSPACE, AND
NUCLEAR ENGINEERING DEPARTMENT
University of California, Los Angeles
Los Angeles, CA 90024
310-825-8275

U.S. STD. THIRD ANGLE PROJECTION

External mirror   Power supply

LASER OPERATING

Light sheet   Jet exit   Camera   Beam canopy

Figure 2.5   Photo of Illumination and Image Acquisition Subsystems

thus reduce reflected light off the FTF surface. A 300-mm focal length cylindrical lens (4) at the front of the canopy acts to thin the sheet so that its vertical divergence is kept to a minimum.

II.2 The Image Acquisition Subsystem

Iodine will fluoresce at wavelengths somewhat greater than 532 nm (e.g. in the yellow). As noted above, some previous 532 nm work at Sandia [20] has shown that visible fluorescent intensities can easily be generated using about 10^{16} molec/cm^3 I_2 and energy densities of about 150 μJ/cm^2. The I_2 number density here is a factor of 10–100 times that for our jet exit conditions. Nevertheless, we can see visible fluorescence against a dark background, and as previously mentioned, obtain a satisfactory signal in the presence of room or outdoor light with an intensified camera.

We use an ITT image intensified solid-state CCD camera F4577. It incorporates a Generation II image intensifier, an 11-mm CCD sensor, and integrated electronics to produce a very high resolution RS-170 video signal. The image intensifier uses a microchannel plate (MCP) current amplifier with an S20 photocathode. The CCD is a Texas Instruments TC241 488(V) × 754(H) pixel, frame-transfer device with a 6.6 × 8.8 mm image format. The electronics provide photocathode gating, gain control, and an automatic iris control signal. The F4577 uses a tapered fiber optic coupling between the intensifier and CCD to achieve a high-efficiency image transfer.

Background light is rejected using a Melles-Griot Interference filter centered at 550 nm with a 40 nm half-width. Other interference or band-pass filters or a combination thereof may be employed as necessary.

The contribution of unfiltered background radiation to the signal is drastically reduced by gating the camera ON only during the interval the jet is illuminated (e.g. for 6 ns each laser pulse). This is the primary function of the image intensifier. It is not possible to gate the high voltage supply that drives the intensifier as fast as 6 ns, but 100 ns is possible. This effectively changes the integration period for background radiation from approximately 20 ms to 100 ns, suppressing the background by a factor of 200,000. Since the fluorescence may also be amplified by a factor up to 10,000, both factors together result in a huge increase in signal-to-noise. The images from the camera are down-linked and recorded for later analysis.

The camera, which measures 10.1 in. × 4.7 in. × 3.3 in., is located in the front portion of the internal components rack near the jet exit (Figures 2.4–2.6). The jet fluorescence is imaged onto the intensifier focal plane using a system of one internal and one external mirror, along with a standard Nikon 28 mm f2.8 camera lens on the F4577. The internal mirror is oriented at a 45° angle and mounted just above the camera lens, allowing an outward view. The 45° external mirror is secured to the side of the ICR, and allows an overhead view of the jet trajectory plane. This arrangement results in a viewable area of about 11.5 × 16.6 cm in the plane of the jet. The field of view is depicted in Figure 2.7, along with expected jet trajectories at M_{jet} = 1.0 and free-stream Mach numbers, M_∞ = 0.8 and 1.4. Higher M_{jet}s will give greater penetration and will use a

Figure 2.6 Forward Section of the ICR
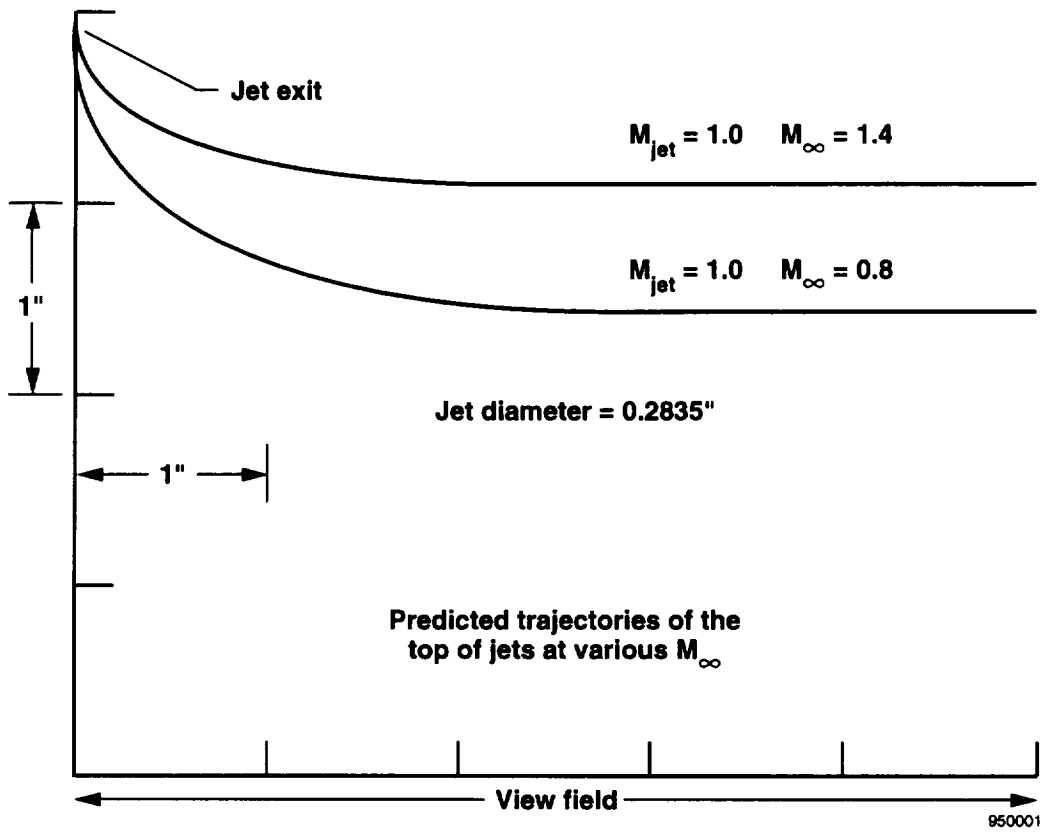
Figure 2.7 Field of View of Camera

Jet exit

$M_{jet} = 1.0$ $M_\infty = 1.4$

$M_{jet} = 1.0$ $M_\infty = 0.8$

1"

1"

Jet diameter = 0.2835"

Predicted trajectories of the
top of jets at various M_∞

View field

950001

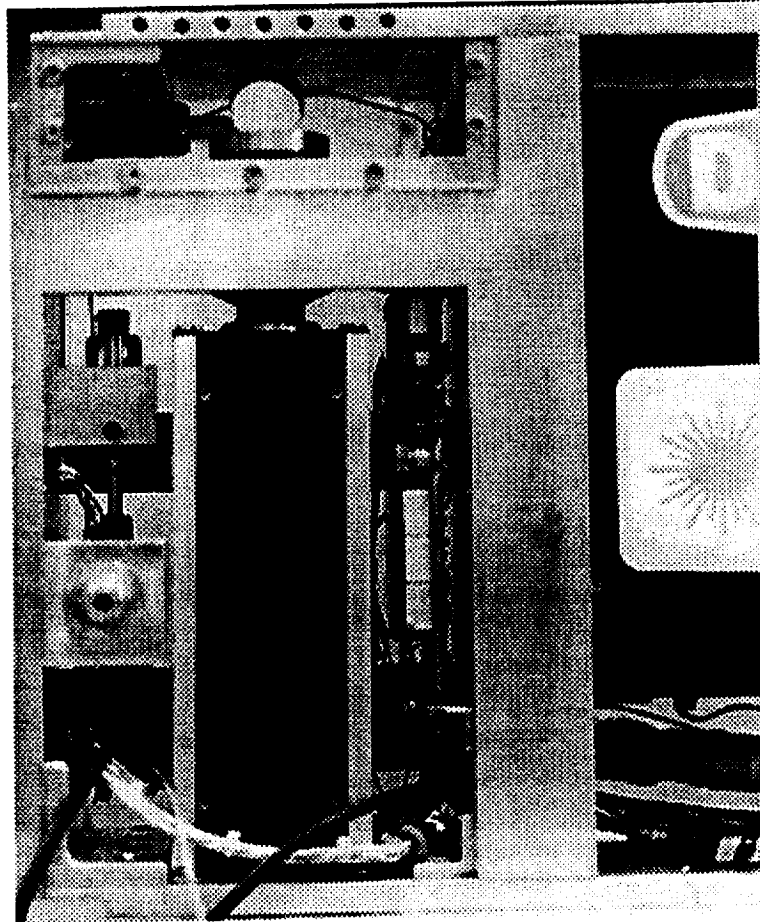greater portion of the viewable area. [Due to the recent addition of a mirror guard, the viewable area may be slightly smaller; but this will not pose a problem.] Additionally, the external mirror will not disrupt the flow in the region of the jet, due to its thinness (essentially 2D), inclination, and distance some 12 in. above the jet exit. Shocks off the mirror edge do not coincide with the trajectory of the jet. A Plexiglas window is mounted on the ICR and separates the inner and outer mirrors. It is positioned flush with the outer skin of the FTF side panel.

II.3 The Jet Subsystem

A schematic of the apparatus used to handle and form the jet is given in Figure 2.8. Photographs are shown in Figures 2.9–2.10. Nitrogen, stored at pressures up to 3000 psig in a high pressure reservoir 5.1 liters in volume, is used to form the jet. The reservoir/tank is flight-certified by NASA and was last pressure tested in June 1992. To conserve nitrogen, the jet will be operated intermittently at preprogrammed intervals by activating a solenoid valve. The valve is a Burkert Type 256 2/2 way, direct-acting, normally-closed solenoid valve. Normally-open valves may be used for safety reasons, but continuous power will be needed, since the valve must be usually closed. Also, normally-open valves tend to have comparatively longer opening and closing times than normally-closed valves.

When the valve is activated, nitrogen flows through a single pressure regulator previously adjusted to provide the desired pressure P_{exit} at the jet nozzle exit for some target altitude and Mach number. The regulator, by Fisher Scientific, is a two-stage type, which allows accurate downstream pressure regulation essentially independent of upstream reservoir pressure. The first stage reduces the pressure by 90 percent, and the second stage regulates the remaining 10 percent to the selected pressure value. To create a perfectly expanded gas jet at other target Mach numbers, the F-104G will cruise at different altitudes to obtain the correct p_∞. Communication between the pilot and control tower will also facilitate the appropriate flight paths. (See Figure 1.8 for a closer look at the flight plan.) For the first sequence of experiments ($M_{jet} = 1.0$), the downstream pressure of the regulator will be set to approximately 64,900 Pa (9.42 psia). This will produce the desired P_{exit} of 39,000 Pa (5.66 psia). Due to the Joule-Thompson cooling from the extreme pressure drop across the regulator, a heater is required to heat up the gas prior to mixing with the iodine vapor. The "preheater," as it is also known, is a Hejet heat-gun element that draws 7.8 A, generating 858 W at 110 VAC, supplied by the aircraft. The heat-gun element is installed inside a modified Whitey 300-cc stainless steel sample cylinder. A sufficiently high temperature must be maintained at the jet exit in order to prevent condensation of the iodine seed. It also increases the population of the high ($50 < j < 100$) rotational states that are accessible at 532 nm. This is achieved by wrapping the jet line between the preheater and jet exit with heating tapes. The heating tapes, made by Omega Engineering, are insulated with Samox® (registered trademark of Brisk Heat Corp.) yarn and can be exposed to continuous temperatures of 1400 °F (760 °C); heating tape burnout should not be a problem. Exit temperatures in excess of 373 K are common with the current preheater-tape combination, though exact temperatures are dependent on preprogrammable run times (which vary from 6–13 sec).

After preheating, the nitrogen passes a flow-control orifice 4 mm in diameter, made of stainless steel. Iodine vapor is then seeded into the main nitrogen flow at a T-branch. The

32
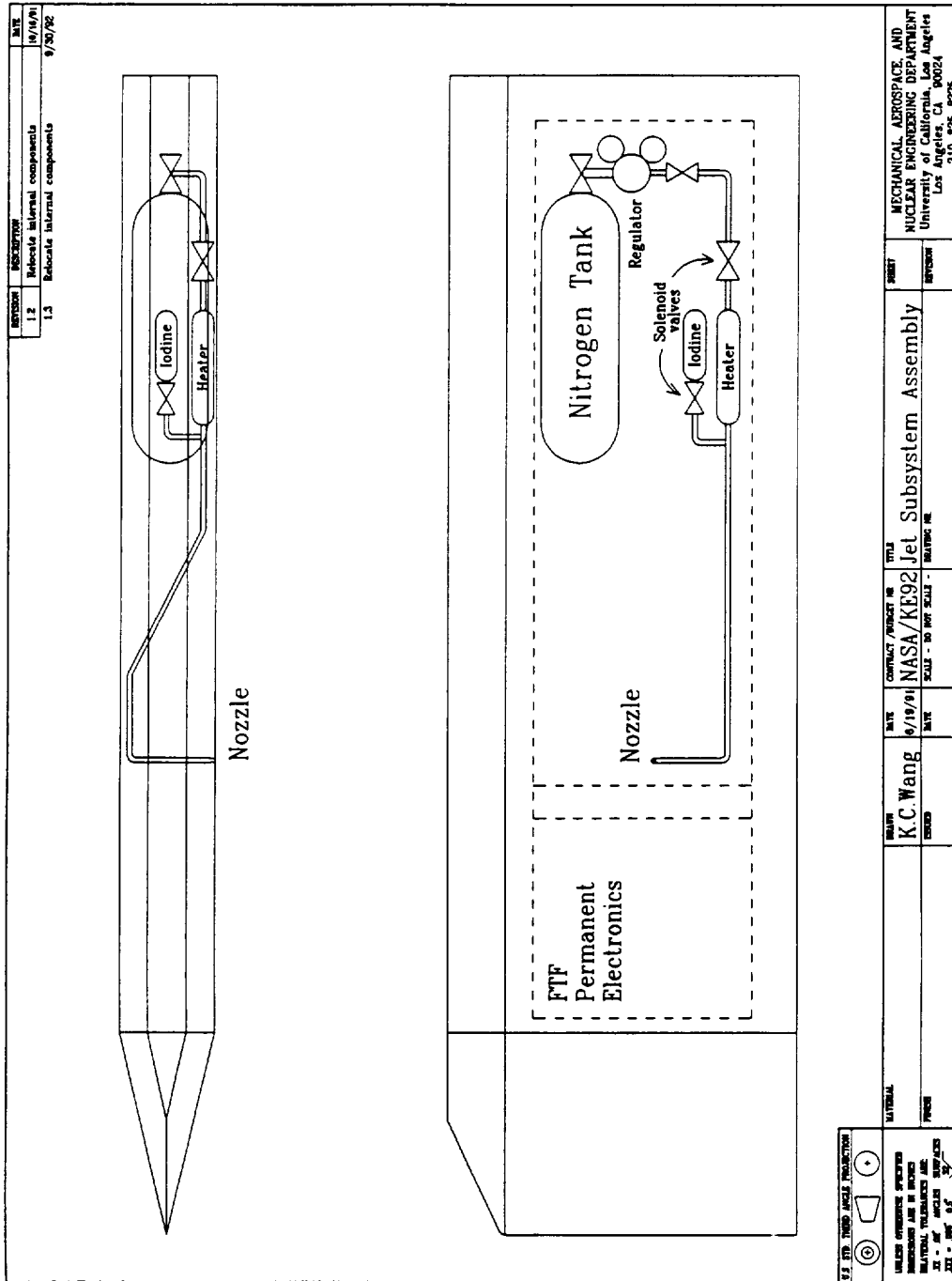
Figure 2.8 Schematic of Jet Formation Subsystem

Nozzle

Iodine

Heater

Nitrogen Tank

Regulator

Solenoid valves

Iodine

Heater

Nozzle

FTF Permanent Electronics

Jet Subsystem Assembly

K.C.Wang

NASA/KE92

MECHANICAL, AEROSPACE, AND
NUCLEAR ENGINEERING DEPARTMENT
University of California, Los Angeles
Los Angeles, CA 90024
310-825-8275

REVISION	DESCRIPTION	DATE
1.2	Relocate internal components	10/16/91
1.3	Relocate internal components	9/30/92

Figure 2.9   Photo of Jet Formation Subsystem

laser
optics

right side of
laser head

iodine
reservoir

iodine
line to
valve

nitrogen
fill valve

heater
controllers

pressure
regulator

nitrogen
line

pressure
transducers
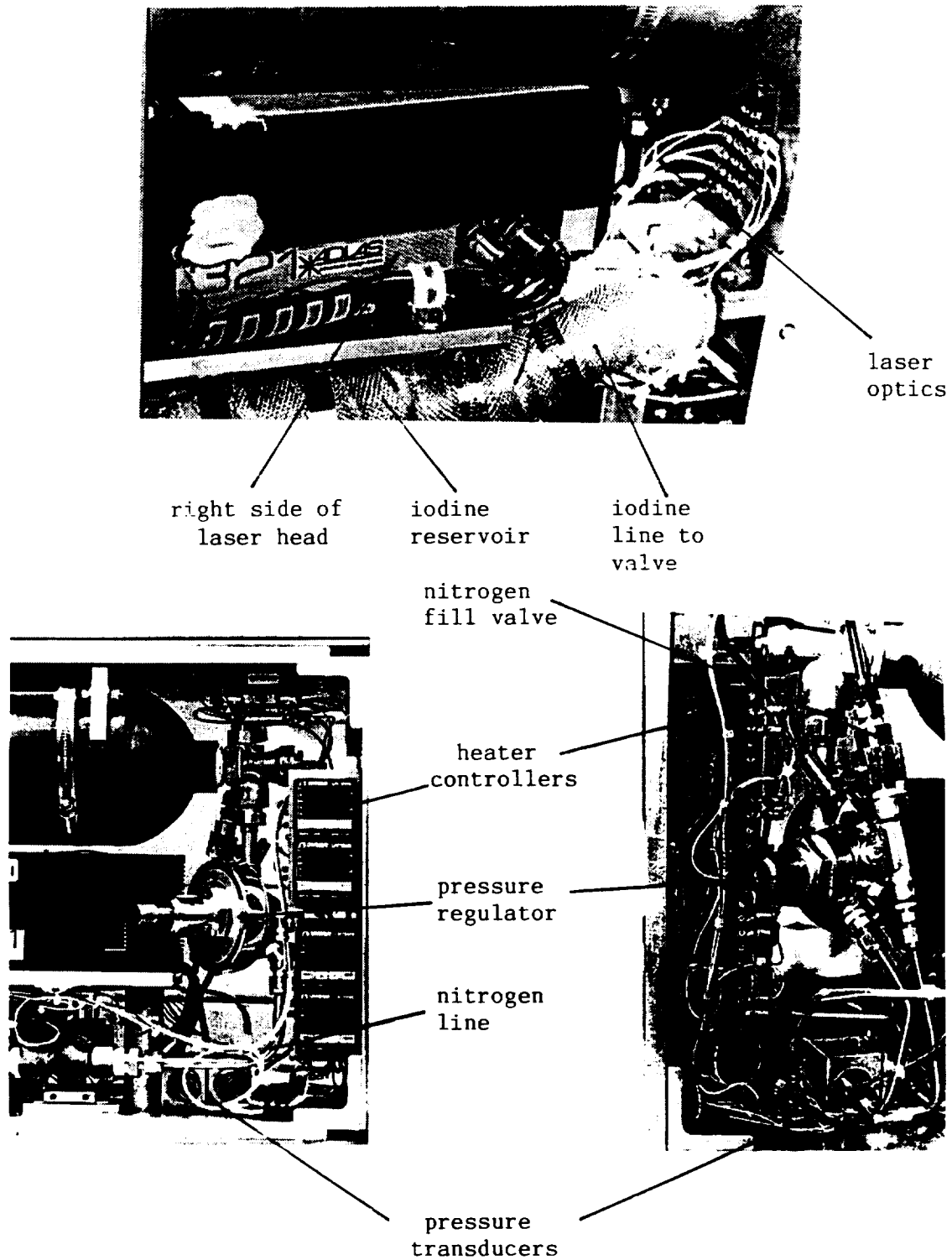
Figure 2.10   Alternate Views of the Jet Formation Subsystem

35

iodine is stored and heated to temperatures of 185–200 °C in a 75-cc Whitey sample cylinder using an Omega Incoloy$^{\circledR}$ (registered trademark of International Nickel Co.) cartridge heater. The cartridge heater, as well as the heating tapes, are controlled by Omega CN76000 series 1/16 DIN auto-tune controllers. All components exposed to iodine are either stainless steel, Incoloy, or Teflon$^{\circledR}$ (registered trademark of E.I. Dupont de Nemours & Co.), to prevent oxidation caused by the iodine. The iodine line and valve leading to the T-branch are heated to temperatures up to 200 °C (or slightly more), raising the vapor pressure to about twice (or slightly above twice) the nitrogen pressure, under target flight conditions. The valve orifice size is 0.116 in. and based on the 2:1 pressure differential, should provide concentrations on the order of 10^3 ppm, suitable for visualization as confirmed by preliminary lab studies. The iodine valve is a General Valve Series 9 two-way, normally-closed solenoid valve designed to handle corrosive materials and high temperatures. It is enclosed in a small aluminum "oven" that provides uniform heating at the valve's designated temperature. Iodine cylinder pressures are very low and do not constitute any pressure hazards. During actual experiments, the N_2 and I_2 valves are controlled automatically from preprogrammed electronics. During purging or filling procedures, both valves can be manually and independently activated/deactivated.

After seeding, the N_2-I_2 mixture is carried in heated stainless steel lines (0.5 in. diameter) and finally passes through an aluminum nozzle to produce a sonic jet at the nozzle exit/throat. The nozzle exit is machined to a diameter of 7.2 mm (0.2835 in.). Different jet exit velocities can be obtained by either readjusting the upstream pressure or by using a different nozzle contour or exit diameter. Information on how to do this can be found in any text on compressible flows, such as Anderson (1990). A summary of the flow properties along the jet subsystem is given in Figure 2.11.

The jet subsystem is pictured in Figures 2.9 and 2.10. Heating elements for the iodine and nitrogen are internal to the iodine reservoir and jet preheater, respectively. Figure 2.9 actually shows the entire ICR with all three subsystems. Figure 2.10 shows selected close-ups of the jet formations subsystems.

The jet subsystem has been subjected to extensive fluid mechanic and thermodynamic analyses as detailed in section I.3.3. The external flowfield around the jet and FTF have been determined numerically considering:

- the oblique shock off the tip of the FTF;
- the expansion fan at the shoulder of the FTF;
- the curved, 3-dimensional bow shock in front of the transverse jet.

In addition, the internal analysis of the jet formation subsystem has been studied using the FORTRAN code FTF2.FOR considering:

- non-ideal, non-isentropic flow from the nitrogen tank past the pressure regulator, with Joule-Thompson expansion cooling;
- a steady-state (approximation), constant pressure, heating process;
- a quasi one-dimensional isentropic flow from the preheater to the nozzle exit.

Copies of both programs, FTF1.FOR and FTF2.FOR are included in the appendix. Both codes were used for preliminary analytical and design studies. Not all subsequent modifications were updated in the programs.

Station #	Temperature (K, C)	Pressure (psi, Pa)
0	293, 20	3000, 20.7E+6
1	261, -12	10.1, 69400
2	365+, 92+	10.1, 69400
3	458+, 185+	14.7+, 101300+
4	473, 200	20.4, 138800
5	423, 150	10.1, 69400
6	423, 150	10.1, 69400
e	345+, 73+	5.66, 39000

Nitrogen Tank

Regulator

Iodine

Solenoid valves

Heater

Nozzle exit

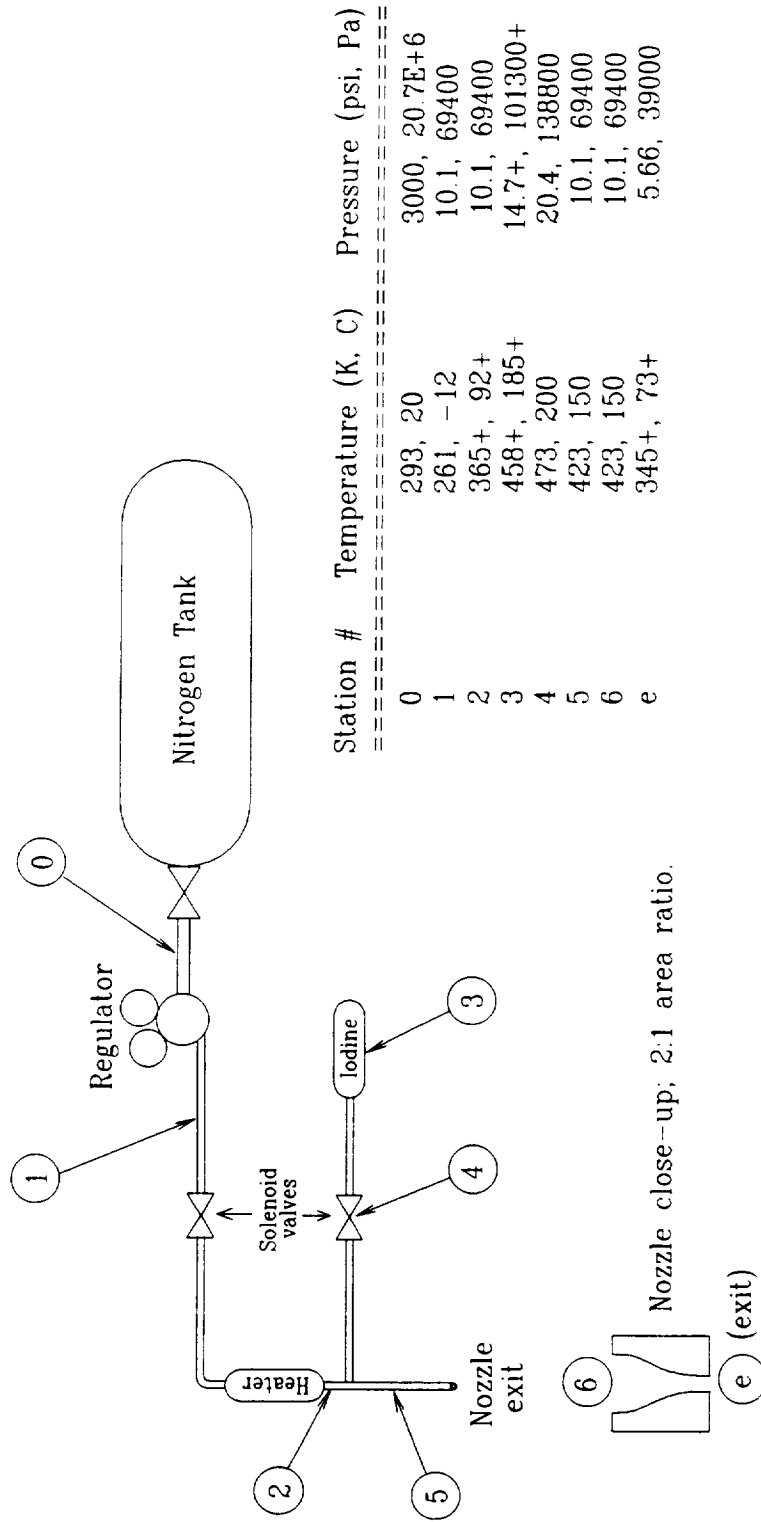Nozzle close-up; 2:1 area ratio.

6

e (exit)

Figure 2.11   Flow Properties Along the Jet Subsystem

Because the F-104G will fly at different altitudes, the jet thermodynamic settings are held constant (and necessarily so). For a typical nitrogen flow of 0.0062 kg/sec (10 l/sec out the preheater), we have enough nitrogen for at least ten 10-second bursts/runs per flight. For a 2000 ppm seeding concentration, the iodine vapor will flow at 1.12 E-4 kg/sec. Since the iodine is stored in condensed form, its supply is not a limiting factor (though at least 10 grams should be allotted per flight).

II.4 ICR Integration and the FTF

Mechanical integration of the three subsystems is facilitated by a unique internal components rack (ICR), depicted in Figure 2.12. The ICR provides expedient access for servicing between flight tests as well as between maintenance at UCLA and delivery to NASA. The ICR is made of aircraft-type 6061-T6 aluminum and bolted together with the use of Heli-Coil inserts. All parts and accessories within the ICR are bolted with Heli-Coil Screw-Lock inserts as well. Heli-Coil Screw-Lock thread inserts positively lock screws and bolts against loosening under impact and vibration by way of an internal, hexagon-like locking thread. In the harsh environment under the fuselage of an aircraft, the effects of both static and dynamic loading on threaded parts are of obvious concern. Screw-Lock inserts meet military specifications for locking torque and vibration (MIL-N-25027 and MIL-I-8846).

When the ICR is fully loaded, it is a completely self-contained unit (minus power lines and signal cables, to and fro) and weighs 118 lb. The center of gravity is located 24 in. from the front edge and 7 1/4 in. from the bottom edge. The ICR fits snugly inside the aft bay of the flight test fixture, where it is appropriately secured. Two side panels, each made of 6061-T6 aluminum, enclose the ICR inside the FTF. The left side panel is 0.25 in. thick so that the nozzle and camera window are flush with the panel, providing a clean flow up to and around the jet exit area. The right side panel is 0.125 in. thick. Both panels are actually mounted in segments of three. The forward panel is continuous from the shoulder of the FTF and extends past the jet exit area, again to provide a clean flow.

The ICR is equipped with several access holes between its three main compartments for flow lines and electronic connections. The laser platform in the aft compartment also serves as the base for the optical canopy. This configuration keeps all laser optics stable and aligned.

Ground vibrations tests have been performed at UCLA to evaluate the ruggedness of the experiment. The ICR, fully loaded, was bolted down to a wooden cart that rolls on four pneumatic tires. The cart was then dragged over several 1 in. × 4 in. wooden planks separated by distances of 2, 3, and 4 ft. The wheelbase of the cart is 3 ft, and the most intense oscillations to the cart were experienced with the planks 3 ft apart. The cart was rolled over this test course several times, with the implied goal of trying to loosen up or shake apart anything that might otherwise loosen up or shake apart while in flight or taxiing on the runway, serious situations to be avoided. The result of the test was that none of the components, electronics, or optics were affected; no visible vibration damage or misalignment was detected. The experiment operated fine after the ruggedization tests.

Unless otherwise specified, all screws: flat head, hex key, steel.

45.625

22.531

7.500

6.000

14.9375

1/4-20 UNC internal threads x32, @ corners.

1.5 x 1.5 x 5/16 angle cut-outs @ 4 corners.

A

A

A - A

1 x 1 x .25 angle beams to support 2 x 6 x .25 channel beam, 13.9375" long.

2 x 2 x .375 angle beams, 6" long. @ 4 corners.

8-32 UNC-2B tap. x16 on channels.

8-32 UNC-2B tap. x16, on top/bot. sides.

0.5" thick Aluminum sides.

REVISION	DESCRIPTION	DATE
1.1	Re-size screws.	10/1/92
1.2	Re-locate channel beams.	9/30/92

U.S. STD THIRD ANGLE PROJECTION

UNLESS OTHERWISE SPECIFIED DIMENSIONS ARE IN INCHES MATERIAL TOLERANCES ARE
.X = .0" ANGLES SURFACES
.XX = .005 0.f 32/

MATERIAL Aluminum 6061-T6		
DRAWN K.C. Wang	DATE 8/19/91	CONTRACT/BUDGET NO NASA/KE92	TITLE FTF Internal Components Rack	"FTF ICR"
ISSUED	DATE	SCALE - DO NOT SCALE	DRAWING NO	SHEET 1/1
FINISH				REVISION

MECHANICAL, AEROSPACE, AND NUCLEAR ENGINEERING DEPARTMENT
University of California, Los Angeles
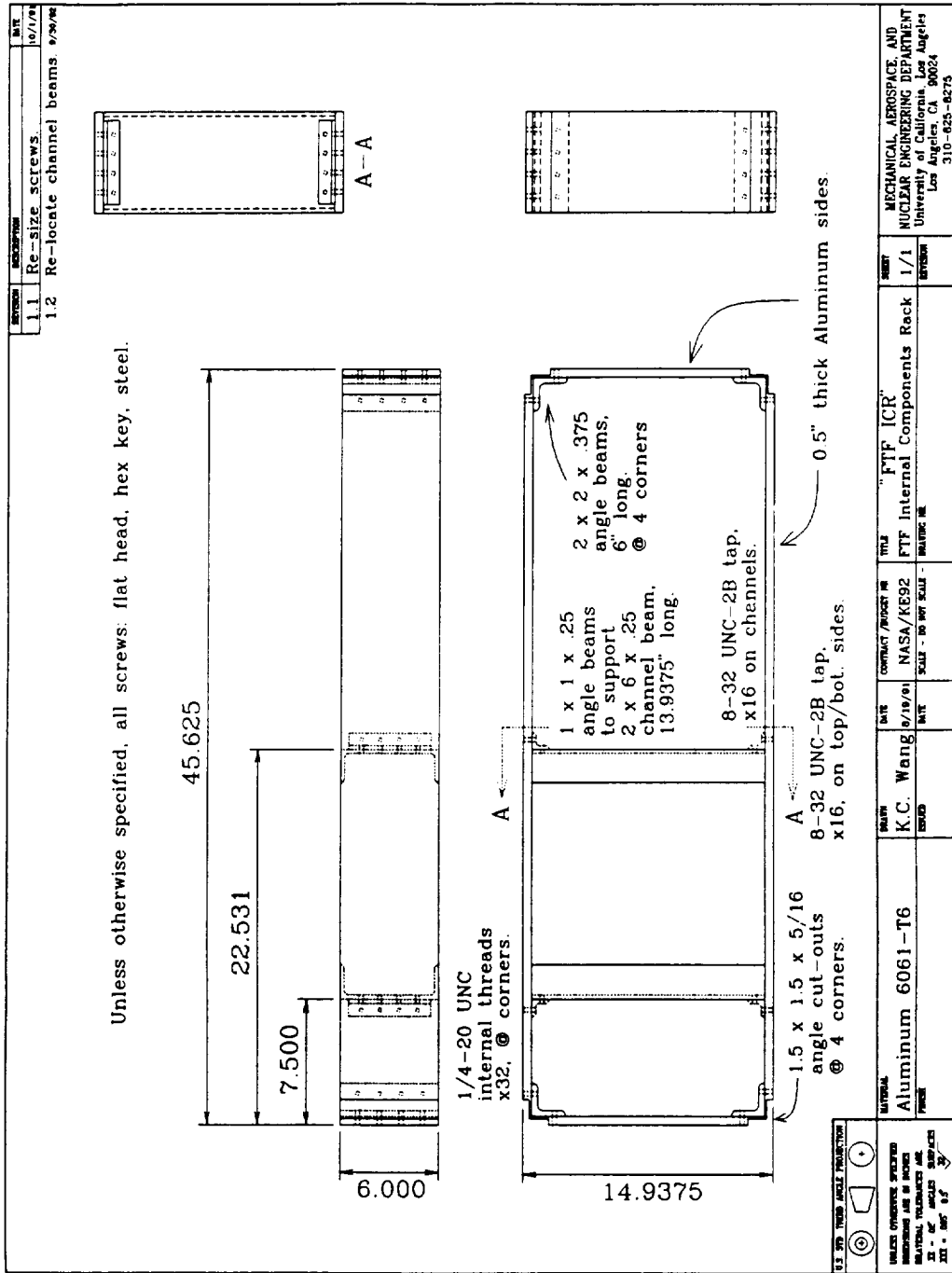Los Angeles, CA 90024
310-825-6275

Figure 2.12 Schematic of Internal Components Rack (ICR)

CHAPTER III
ELECTRONICS AND OPERATING SYSTEMS

III.1 The Electronics Board

The electronics board has two primary functions. It controls the timing of the experiment and also locks out the other heaters when the main jet heater is on. The latter function is necessary to ensure that the 110 VAC load does not exceed 10 A when the jet heater is on. The component and wiring sides of the electronics board are shown in Figures 3.1 and 3.2. Many of the small components are mounted on the wiring side of the board. Schematic diagrams of the circuitry are given in Figures 3.3 and 3.4. Tables describing cable and pin connections are found in the appendix under "Maintenance and Operations."

Power supplies

Power for the electronics is provided by the 28 VDC aircraft power. The circuitry draws about 2 A with the laser and valves off. Actuating the valves draws an additional 1 A. The laser draws a maximum of 1 A. A ±15 VDC switching power supply located on the board provides the voltages necessary for the thermocouple signal conditioners (SC1-4). In addition, there are separate +5 VDC and +15 VDC regulators located on the aluminum bulkhead above the board. The +5 VDC (7805) regulator powers the logic. The +15 VDC (7815) regulator powers the valves, heater relays, the camera and the high current portion of the signal conditioning circuitry. Filtering capacitors associated with the regulators are located on the pin side of the regulators and are potted in RTV. The regulators and associated capacitors can be removed for service as a unit from the board side of the bulkhead. Removing the laser power supply is not necessary.

Aircraft 110 VAC is used to power the temperature controllers and the heaters. The main jet heater (a heat gun heating element) draws 7.8 A. The iodine line and valve heaters (2 heating tapes connected in parallel) draw a total of 2.6 A. The jet line heater (3 heating tapes connected in series) draw 0.9 A. The iodine reservoir heater (a 0.25-in. diameter cartridge heater) draws 1 A. The laser head heating pad draws 0.7 A. The laser head, jet line and iodine reservoir heaters are switched by 3 relays located on the board. These relays (RL1-3) are rated for 2.5 A, 120 VAC resistive loads. The main jet and iodine line/valve heaters are switched by solid state relays located at the top rear of the experiment module. The SSRs are rated for 10-A resistive loads.

The experiment interfaces with aircraft power at the terminal strip located at the front bottom of the module. The 28-VDC and 110-VAC connections are marked. The DC power is grounded to the module frame only at the regulators. If the FTF is part of the aircraft ground plane (presumably it is), hooking up the DC common could result in a minor ground loop.

40
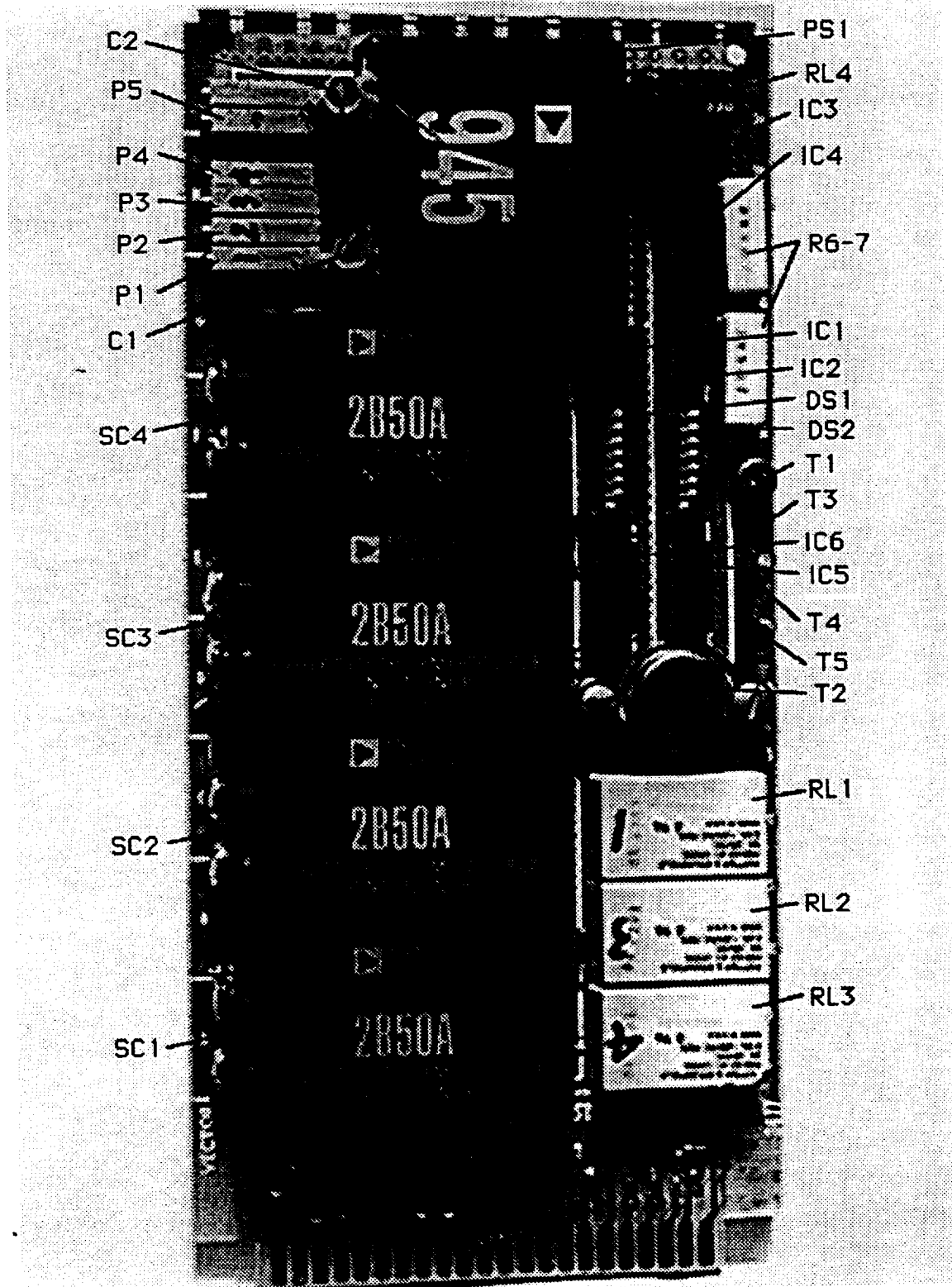
Figure 3.1   Electronics Board (Front)

41
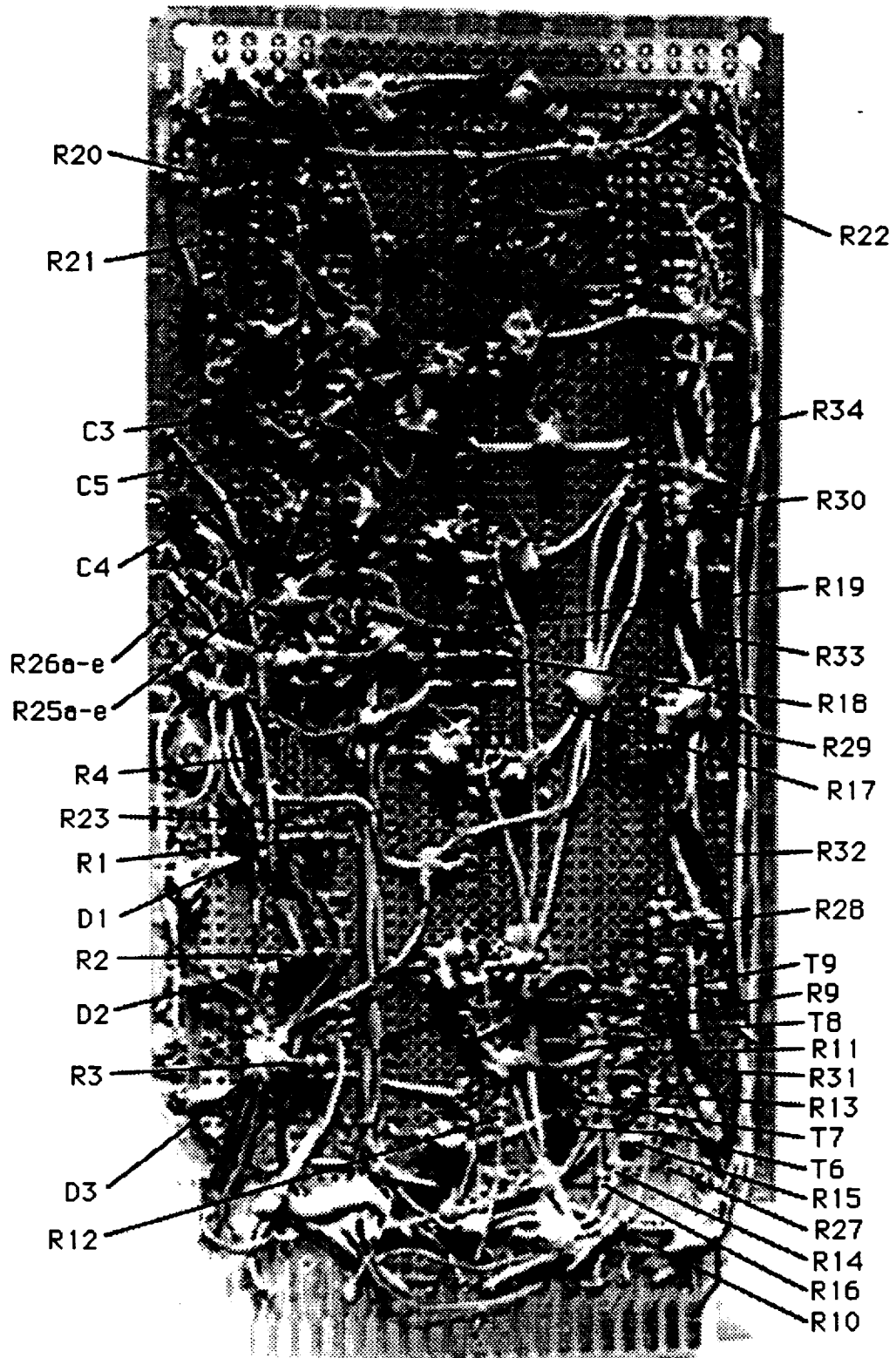
Figure 3.2   Electronics Board (Back)

42

gain resistor

compensation

P1-4 (100)

39

2

3

5

R27-30

tc(+)

tc(-)

21   -15

19

20   +15

2B50A

1

1.82K

40

499

29

28   +15 (from 7815)

8

9

18

17   out

R31-34

1 uf

1 uf

1 uf
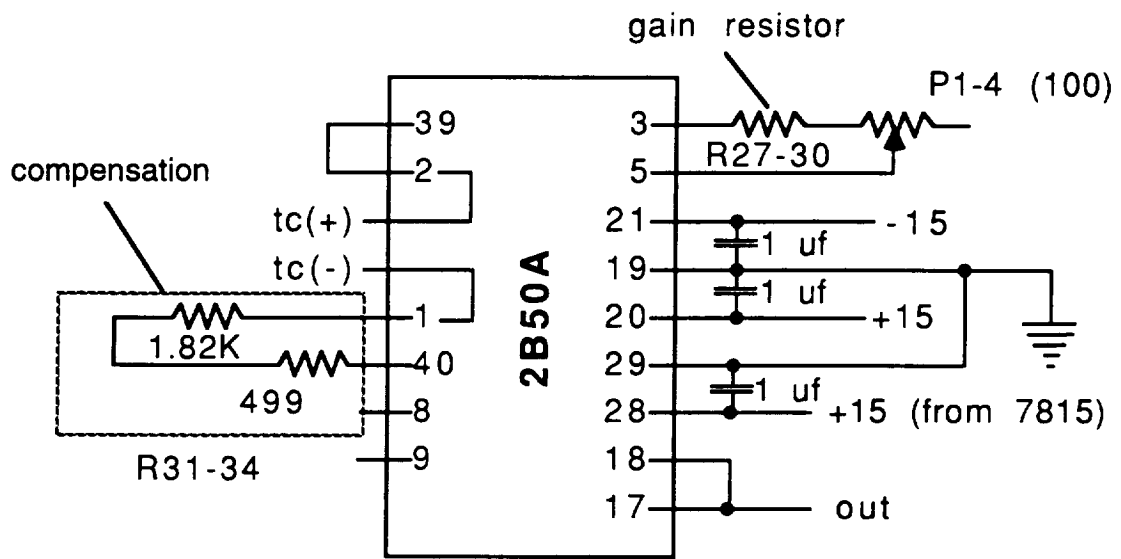
TC	Rg (ohms)
1 & 2	976
3 & 4	239

Figure 3.3   Schematic of Thermocouple Conditioner Circuit

43
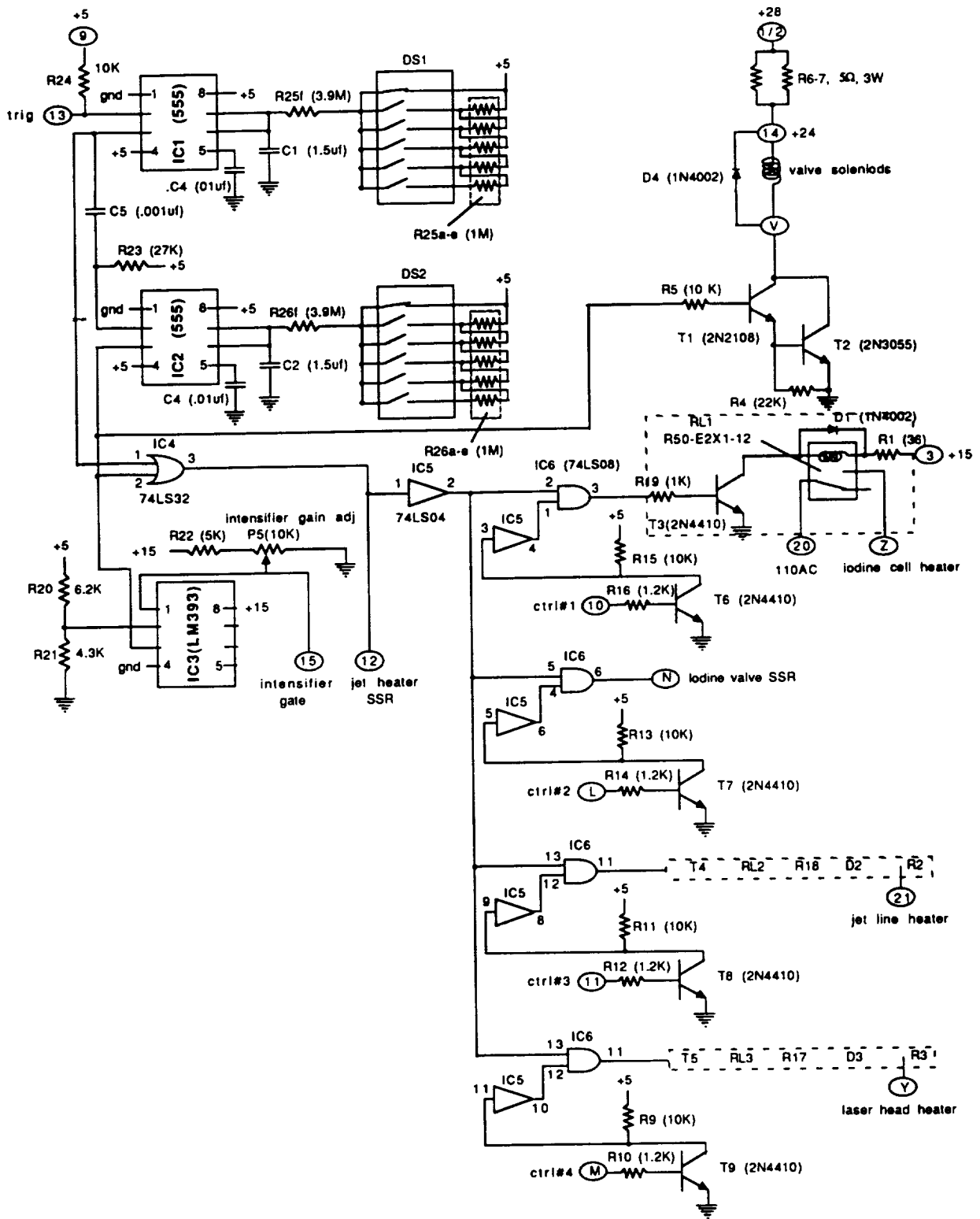
Figure 3.4 Schematic of Overall Electronic Circuitry

44

Timing circuitry

Timing is provided by two 555 timers (IC1-2). The trigger input to the first is held high with a 10 K resistor (R24). Grounding the input (PC edge connector, pin 13) triggers the timer. In our testing this has been done by shorting PC edge connector pins 13 and P, provided as an unterminated twisted pair. The pilot must perform this function each time the experiment is cycled. The output of IC1 goes high on application of the trigger, and stays high for a period determined by the DIP switch setting (DS1). This DIP switch controls the resistance of the RC timing circuit. Only the first 6 switches are used, and only one should be set at a time. Setting switch 1 introduces a resistance of 3.9 M (R25f), providing an interval of approximately 5.8 sec. Setting switch 2 increases the resistance 1 M (R25a), adding approximately 1.5 sec to the interval. Subsequent switches act similarly, so the approximate interval can be calculated by equation 3.1, where "n" represents the number of the switch set.

$$\text{interval (seconds)} = 5.8 + 1.49\,(n - 1) \tag{3.1}$$

Thus, the interval can easily be adjusted from 5.8 to 13.25 sec. Intervals outside of this range can most easily be achieved by changing the timing capacitor (C1). If this is done, a high-quality, low leakage, low temperature coefficient capacitor should be used. A polycarbonate capacitor is currently installed.

The output of IC1 is differentiated (C5/R23) producing a negative going pulse when the timing cycle is complete. This provides the trigger for IC2. The timing circuitry is an exact duplicate of that for the first 555, and is set in the same manner.

The outputs of ICs 1 and 2 are connected to an OR gate (IC4), the output of which drives the main jet heater SSR. The output of IC2 activates the valve solenoids (connected in parallel) through a power Darlington circuit (T1,T2,R22). Thus, the period of the first timer (IC1) controls the warm-up interval of the jet heater. This interval should be set long enough so that operating temperature can be achieved, but not so long as to cause the element to overheat (it is designed for forced convective cooling). We have found the heater begins to glow red hot about 7 sec after power is applied. Repeated operation of the unit with low nitrogen flowrates can cause the jet heater chamber to become hot enough to soften the soft soldered electrical feedthroughs. As the heater chamber is under pressure, this will cause these seals to leak.

The period of the second timer determines the length of an experimental measurement. This should be long enough to let the flow rates and pressures stabilize and the jet to become steady. This interval will have to be selected based on data from the jet exit pressure and temperature transducers during flight tests or in an altitude chamber. To maximize the number of free-stream Mach numbers that can be examined in a single flight, the test interval should be only slightly longer than that necessary to achieve steady state.

45

The output of IC2 also controls the gain on the camera image intensifier. The intensifier is actually gated continuously in synchronization with the laser pulses. The details of the gating will be described subsequently. Since the laser is to be run continuously during a flight, it is important to turn down the intensifier gain when data are not being collected. The gain is set to zero when the jet is not activated, thus prolonging the life of the intensifier tube. A comparator (IC3) increases the gain to a preset level during the interval when the jet is activated. The intensifier gain can be set from 0 to 10 VDC using a ten turn trimpot located at the upper left edge of the board (P5). Counterclockwise rotation will increase the gain. The resulting voltage is most easily monitored by removing IC3 from its socket and measuring the voltage at pin 1.

Solenoid valves

A 24-VDC solenoid controls the nitrogen valve and a 20-VDC solenoid controls the iodine valve. They may be actuated manually or by the timing circuitry, depending on the setting of two switches located at the top of the module near the nitrogen fill line. The left hand switch controls the nitrogen valve, and the right the iodine valve. Either valve may be actuated manually by pressing the respective switch downward. The valve will remain open as long as the switch is held down. This feature is convenient when purging air from the iodine tank. In the neutral (center) position, the valves are disconnected. When the switches are in the up position, the valves are armed (connected to the timer board).

The board circuitry operates the iodine and nitrogen valves in parallel. The 28-VDC aircraft power drops to 24 VDC across two 5-ohm resistors (R6–7) connected in parallel. Another 5 ohm resister drops the 24 VDC to 20 VDC for the iodine valve's lower operating voltage. A clamping diode (D4) is located on the terminal strip at the forward lower part of the module. Current flow to the valves is controlled by a homemade power Darlington (T1,T2,R22).

Controller lock-out

The 0-5 VDC controller output is not directly compatible with TTL logic. Instead, the controller output drives the base of an NPN transistor (T6). The collector is held high by a 10 K resistor (R16). High controller output causes the transistor to conduct, pulling the collector low. The collector voltage is inverted (IC5) and fed to one side of an AND gate (IC6). The other AND input is connected to the (inverted) main jet heater SSR signal. Thus, while the main jet heater is engaged, the AND gate output is low. When the jet heater is off, the AND gate output reflects the controller output. In most cases, the AND gate output drives the base of the transistor (T3) that switches the 110 VAC heater relays. The relays are powered from the high current +15 VDC supply, which drops to the +12 VDC relay coil voltage across a 36 ohm resistor (R1). The hot side of the 110 AC is connected to the common of the SPDT relay (RL1). The heater element is connected to the normally open contact. Thus, when the controller output is high, the heaters are engaged. The other end of the heater is connected to the 110 AC common at one of the terminal strips.

Laser relay

Provision is made for activating/deactivating the laser from the cockpit. The laser power supply will activate when the 28-V power is applied, but the laser itself will not turn on. The laser is turned on remotely by shorting pins 8 and J on the PC card edge connector, thereby applying 5 volts to the coil of relay RL4. Access to these pins is provided as an unterminated twisted pair. Energizing the relay is functionally equivalent to depressing the reset switch on the front panel of the laser, toggling the laser between the off and on states. The laser may take a few seconds to turn on after the relay is energized.

Thermocouple signal conditioners

The thermocouples are conditioned by Analog Devices 2B50A signal conditioners. All the conditioners are configured to compensate type E thermocouples. The compensation is set by the 1.87 K resistance (R27–30) between pins 1 and 40. The conditioner gain is set by the resistance (R31–34) between pins 3 and 5. In each case we utilize a low temperature coefficient metal film gain resistor in series with an 100 ohm trimming potentiometer (P1–4). For conditioners 1 and 2, connected respectively to the iodine reservoir and iodine valve thermocouples, a 976-ohm gain resistor is used. The trimpot is set to provide a voltage gain of 200 at the output (pins 16–17). Conditioners 3 and 4 are connected respectively to the jet line and jet exit thermocouples. The gain resistors here are 239 ohms, and the trimpot is set to provide a voltage gain of 700. The trimpots were set up using the actual thermocouples immersed in boiling water.

Camera gating

The camera gating is controlled by added circuitry (Figure 3.5) inside the camera case. This circuitry has been inserted between the External Gate Input BNC connector and the cable originally attached to it inside the camera. The sync output from the laser is connected to the External Gate Input BNC. The sync output falls upon activation of the Q-switch, with the laser pulse occurring a few nanoseconds later. The inverted sync pulse (IC7) drives the input of a dual monostable multivibrator (IC8). The first multivibrator controls the delay between the fall of the laser sync and the start of the intensifier gate. The falling output of the first multivibrator triggers the second, which controls the width of the gate pulse. The output of this multivibrator is inverted and used to gate the intensifier power supply.

The gate pulse width is set by potentiometer P7 to 120 ns, the minimum gate width specified for the intensifier power supply. The delay between the fall of the Q-switch and the laser pulse ranges from 620–1100 ns, depending on the laser pulse energy. The approximate delay for different power settings is given in Table 1. The delay can be adjusted by means of P6. It is currently set for 570 ns, ensuring that the intensifier is gate on during the 20-ns duration of the laser pulse at full power. As long as the laser is operated at full power, there will probably be no need to change the gate or delay settings. If changes need to be made, both the delay and gate potentiometers can be accessed without removing the camera case. However, we have not provided access to the gate output. This oversight

47
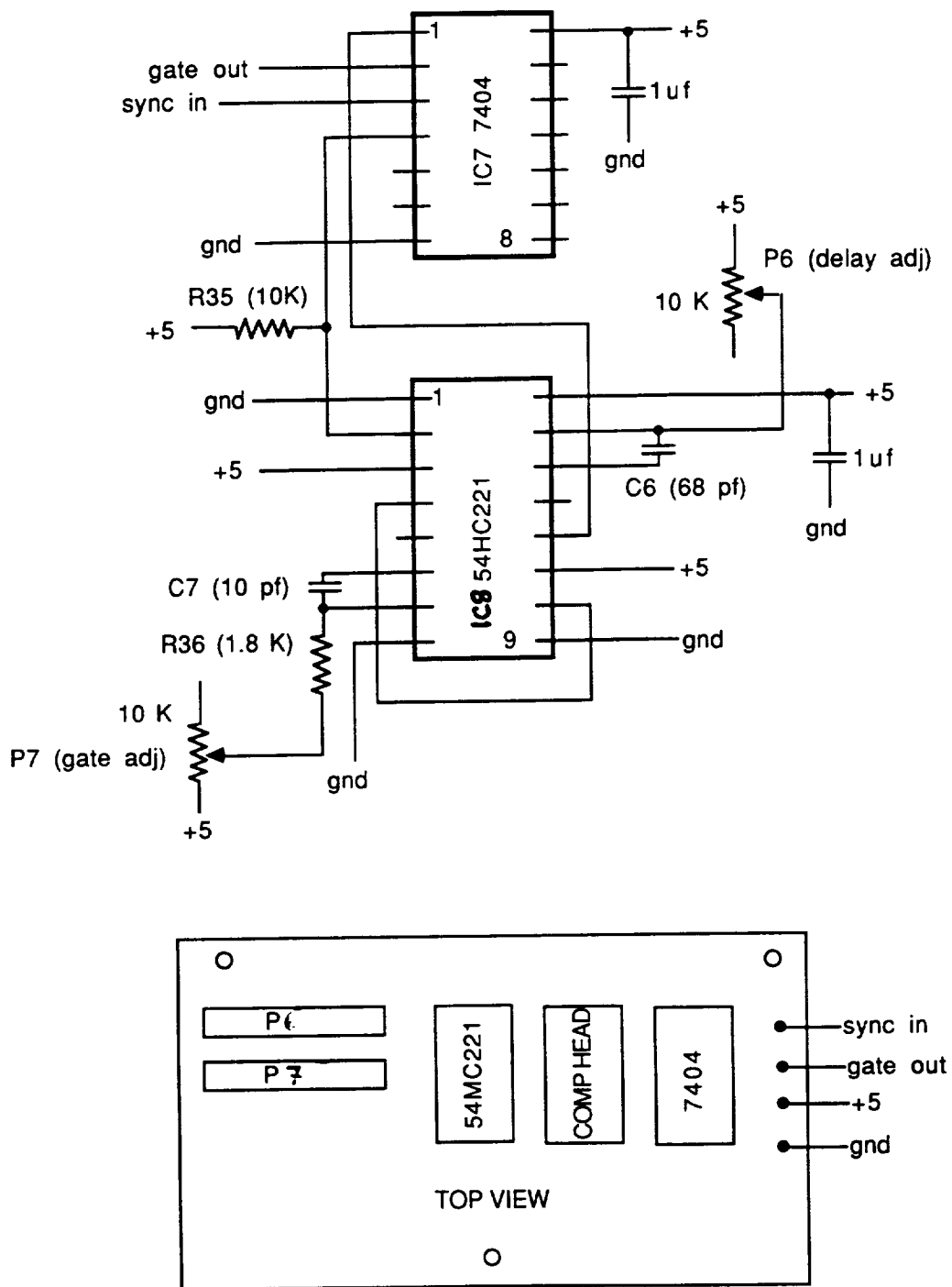
Figure 3.5 Schematic of Camera Gating Circuit

means that the camera case will still have to be dissembled. An easily accessible test point for the gate output should be added. Possibly this could be accomplished by drilling a small hole in the camera case opposite the gate out pin located at the side of the PC board.

When not in use, the two small potentiometer access holes in the camera case should be covered by a piece of black tape to prevent light leaks. This would also apply to any access hole made for a gate output test point.

Table 1. Approximate relationship between Q-switching and
laser output as a function of laser power

Power (%)	Delay (ns)
6	1100
14	900
54	700
98	620

III.2 In-Flight Operating Procedure

During actual in-flight experiments, the operating procedures are purposely straightforward and simple. Such an arrangement is necessary due to the limited amount of activity the pilot can perform outside of flying the aircraft itself. Ground-based maintenance, operation, and testing are more involved and is only briefly mentioned below and detailed in the appendix.

By having the complete experiment inside the relatively thin (low-drag) FTF, we plan to achieve speeds up to $M_\infty = 2.0$. As mentioned previously and outlined in Figure 1.8, we are also interested in running tests at Mach numbers: 0.8, 1.0, 1.2, 1.4, 1.6, 1.8. If the F-104G/#826 cannot achieve Mach 2 in level flight, it will have to dive from a higher altitude and then attempt to hold the right altitude at Mach 2 for the few seconds needed for the test run. Because we cannot reposition the laser sheet in flight, all tests within a given series of flights must be conducted at a fixed angle of attack (about +3°).

In preparation for a flight test, the ICR must be secured inside the FTF. Both 110-VAC and 28-VDC power should be supplied to the experiment prior to "buttoning-up" with the FTF side panels. All four heater controllers should be confirmed on and controlling their respective heaters as tuned. Upon power up, the laser power supply and electronics board will also be on/armed. This power-up preflight check should be done no earlier than 60 min to takeoff as the heaters must stabilize to the set points. Of course, all other components must be functional and flight ready. When all systems are checked out, the FTF side panels may be secured and the aircraft may proceed to taxi onto the runway.

49

The pilot has a series of concise tasks directly involved with the experiments, although in effect, he is only required to press two buttons/switches at the proper times.

(1) Upon takeoff, activate laser. Laser begins to stabilize.

(2) Fly above target altitude at predetermined Mach number; cf. Figure 1.8.

(3) Begin descent through target altitude, trying to maintain target speed. Activate experiment: nitrogen preheater is fired on first for a preprogrammed interval; then, appropriate valves open and camera gated for a given interval. Ideally, the middle of this interval will occur when the aircraft is at target conditions.

(4) When valves and camera are on, pitch a few degrees above and below +3 alpha, the typical alpha for F-104G cruise, to ensure the gas jet intersects with the laser sheet.

(5) Verify with tower successful downlink of images.

(6) Proceed to next target condition.

(7) Iterate (2) through (6) as needed and as allowable.

(8) After experiments, deactivate laser prior to landing.

Operators and experimenters will monitor the experiments and communicate with the pilot during the tests from the control tower at NASA Dryden. Target flight conditions will be confirmed with the use of aircraft-equipped pressure pitot probes. Signals from pressure transducers and thermocouples inside the experiment will provide necessary and sufficient data to help monitor the tests. Video signals (RS-170) downlinked from the camera will be seen in real-time as well as recorded on a ground-based VCR (Beta) for later analysis and processing. If images are unacceptable (either too faint or nondetectable), the following troubleshooting procedures should be performed, assuming obvious failure is not evident yet.

(1) Confirm left (experimental) side of FTF is facing away from sun, assuming flight is in daylight. Confirm reflected sunlight from clouds is not too bright to drown out fluorescence signal.

(2) Radio pilot to repeat same experiment.

(3) If fluorescence is not visible at all, even at foot of jet orifice, radio pilot to return to base; proceed to step (5). If some fluorescence at foot of orifice is visible, proceed with step (4).

(4) Request pilot to hold best alpha for full trajectory fluorescence during experiment, as determined by downlinked images, regardless of altitude or speed drift away from target conditions. Continue on to other experimental conditions as possible.

(5) If no fluorescence is detected in flight, land plane and begin inspection of all three subsystems for proper alignment and operation. Also inspect electronics board.

(6) Process obtained images on computer-digitizer to detect any faint images.

(7) Run ground tests in environmental chamber as necessary, under simulated flight conditions (pressure and temperature) wherein the experiment failed.

(8) Correct area(s) of failure as found, and re-fly experiment as per previous in-flight procedure.

(9) If no clear failure is found, fly at night to eliminate background daylight noise factor. This option is possible, but logistically difficult due to scheduling and manpower problems inherent in night (after-hours) flights.

CHAPTER IV
DEVELOPMENT OF RESULTS

IV.1 Methods of Analysis

Upon completion of a successful series of flight tests, data from three separate sources must be considered:

(1) Aircraft speed, altitude, and pressure readings.
(2) Experimental temperature and pressure readings from the jet subsystem.
(3) Recorded video images of the transverse gas jet.

Data from all sources are interrelated based on their time dependence. Thus, it is important to interpret video images in light of the data from sources (1) and (2).

Images, stored on Beta tape format, will be computer processed and digitized to maximize visualization. Using the facilities of UCLA's Office of Academic Computing (OAC) Visualization Laboratory, several techniques are available, used either alone or in combination, to generate highly refined and informative images. The process involves transforming (rasterizing) the field data into pixel values. From there, the raw raster image (of pixels) can be processed using such packages as AVS, Photoshop, NCSA Image, NIH Image, or PV-WAVE.

Once an acceptable processed image is obtained, the image can be analyzed in two general respects: (1) Qualitatively, the geometric trajectory and spreading of the gas jet; including upper and lower boundaries, jet curvature, penetration distance/height, downstream distance until zero curvature, extent of mixing with air along the jet. (2) Time-dependently, the rate of spreading and mixing from the initial "burst" to the stabilized jet flow; would require making real-time video "movies."

IV.2 Previous Data and Model Predictions

Processed images can then be compared with previous data and model predictions. Previous experimental data for the momentum ratios tested in this study are limited in availability, which of course is one reason why these momentum ratios were tested. Gas jets in crossflow velocities of $M = 0.8$ have been obtained by Manela and Seginer (1986). A few data points for $M = 1.38$ are found in Orth et al. (1969) and for $M = 1.4$ in Lee et al. (1992). Other data are for Mach numbers of 2.0 and greater, and usually for cases with severely underexpanded jet; thus, they are not of great interest here. Outside of these previous experimental results, we must depend on computational/analytical results. To this end, we can run the appropriate numerical code [Heister and Karagozian (1990a)] at the exact momentum ratio and thermodynamic conditions corresponding to a particular set of images obtained in flight. Direct comparisons of qualitative features can be made in terms of the characteristics outlined above in section IV.1. Examples of some numerically

generated transverse jet trajectories are shown in Figure 4.1. The upper figure depicts predicted trajectories for three jet-to-free-stream momentum ratios based on the Heister and Karagozian (1990a) model. The lower figure shows trajectories for the same three momentum ratios according to the code developed by Le and Karagozian (1992). Researchers performing experimental work on transverse jets include R.K. Hanson at Stanford University and J.C. McDaniel at the University of Virginia, Charlottesville.
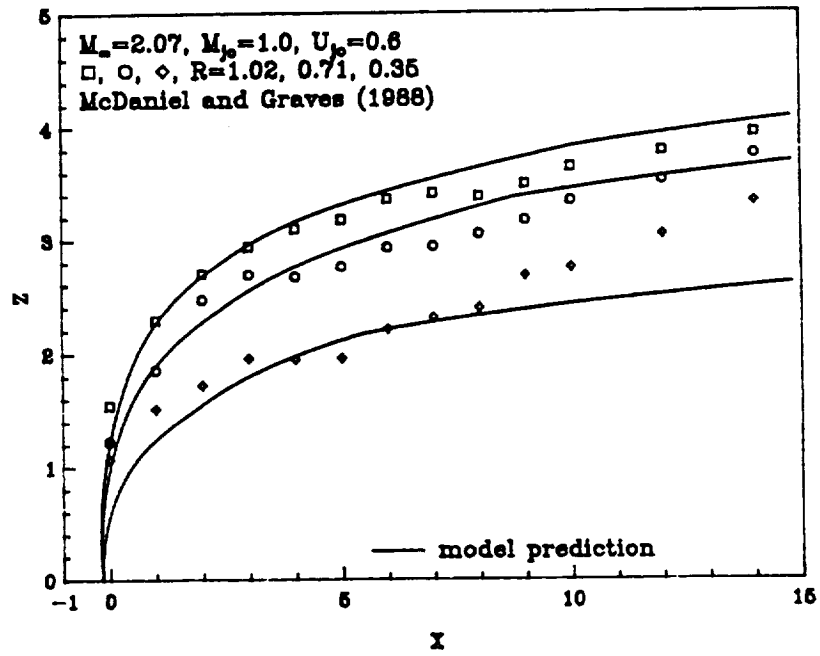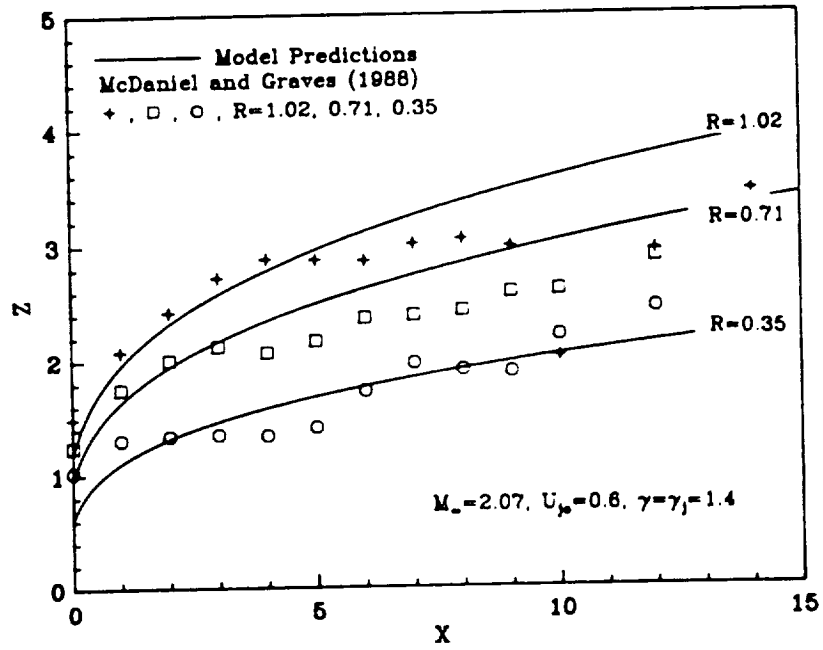
Figure 4.1   Previous Transverse Jet Data, Analytical

CHAPTER V
CONCLUSIONS

V.1 Summary

We have presented the detailed design and development of a unique flight test experiment to study nonreacting gas jets injected into a range of transonic and supersonic crossflows. Two preliminary design codes have been developed to predict fluid and thermodynamic conditions of the experiment while in flight. The desired situation is to form a properly regulated, heated, and seeded nitrogen jet that is either perfectly expanded or slightly underexpanded upon exiting the nozzle. The results of these codes also provide guidelines for the procedure in which the flights are to be conducted. The method of flow visualization is to apply planar laser-induced fluorescence (PLIF) with a Nd:YAG laser into the planned flight environment. Images will be recorded with a gated intensified camera equipped with appropriate optical filters to capture the fluorescence. Laboratory tests have been conducted to determine adequate iodine seeding concentrations using a specially designed optical [iodine] reference cell. Other tests have measured the fluorescence spectrum of iodine under the 532-nm light of the [frequency doubled] Nd:YAG laser. The results summarized above are detailed in sections I.3 through II.3.

A highly compact and rugged internal components rack (ICR) has been designed and built to integrate and carry the parts and instrumentation necessary for experimentation. While entirely enclosed within this rack, PLIF of an iodine-seeded nitrogen jet with a cross-sectional diameter of 7.2 mm has been successfully imaged using a gated intensified camera (at sea level conditions). A thoroughly integrated electronics board has been designed and wired to control the experimental run sequence; operate the heaters, valves, and laser; and monitor/downlink critical temperatures and pressures within the jet formation subsystem. The result is a simple two-button system of operation for the pilot to perform when at target flight conditions. (PLIF and intensified camera imagery were never meant to be this easy!) The main difference between sea level and flight conditions will be the vibrations from the aircraft engine, the cooler ambient temperature, and the lower ambient pressure. A series of vibration tests on the ground have shown no appreciable affect on the experiment, in particular, the optical alignment. The lower temperature and lower pressure are actually favorable for they respectively cool the electronics and create the proper back pressure behind the nozzle for the perfectly expanded jet. Power supplies and sources have been appropriately potted to prevent high-altitude arcing. Thus, as long as the pilot can hold the predetermined flight plan and angle of attack, in-flight PLIF and jet imaging will be successful. Some adjusting of the pressure regulator may be necessary due to the pressure differential at altitude, but this and other minor adjustments are nothing a thoughtful effort at trial-and-error cannot solve.

V.2 Future Work

Upon successful completion of this first phase of in-flight flow visualization experiments, numerous other fluid mechanics phenomena can be studied. Essentially, we will have pioneered the use of traditionally ground-based laser diagnostics and imaging

techniques to fully realistic in-flight environments. The proverbial door will be wide open to using the "flying wind-tunnel concept" where realism, versatility, and cost-effectiveness will be the hallmarks. Limitations of test section area, improper scaling of noise and turbulence levels, opposing wall effects, and narrow Mach range that are inherent in most terrestrial wind tunnel facilities will either be greatly minimized or nonexistent.

The immediate extensions of the jet trajectory work to other geometries of practical interest are straightforward. Examples include injection behind a rearward-facing step, injection of multiple or staged jets, injection through slot or elliptical nozzles and at various exit Mach numbers, etc. The use of liquid jets in the original, or many of the alternative configurations, is also of interest. The rearward-facing step problem is of particular current interest. The situation is sketched in Figure 5.1. Previous wind tunnel tests [McDaniel and Graves (1988)] in this geometry have examined jet penetration with respect to injector locations downstream of the point at which the shear layer reattaches to the wall. Recent calculations by Le and Karagozian (1992) indicate that if the injector location were moved upstream of this point into the recirculation region, it should be possible to double the jet penetration. There is currently no experimental data available to confirm this. If it is true, however, injection at this location should provide much better mixing in a scramjet or other application requiring efficient and thorough mixing. Flight tests could provide the experimental data necessary to validate this approach. The instrumentation developed for the current program could be used with only minor (mostly external) modification.

The present aircraft for our experiments, NASA's F-104G/#826, is ideal for in-flight experiments because of the extensive amount and broad range of in-flight work it has already accomplished. Although this aircraft will be retired within the next year, another is scheduled to take its place, dubbed the "F-15B Aerodynamic Flight Facility." The McDonnell-Douglas twin-seat F-15B is a high-altitude, high-speed (over Mach 2.5) fighter aircraft. It is also equipped with a newly designed and built "Advanced Flight Test Fixture (AFTF)," similar to the current FTF, to carry and conduct aero/thermo/fluid dynamic experiments. In addition, NASA Dryden has recently acquired two Lockheed SR-71As and one SR-71B for use as supersonic/hypersonic research facilities [Urie and Lux (1992)]. The SR-71 is, for sustained flight, the highest flying, fastest aircraft in the world today, with cruising altitudes of 85,000 ft and speeds of Mach 3+. We are very interested in the external burning experiments slated for the SR-71 (the future budgetary state of the project is uncertain). Several diagnostic approaches are possible, based on the proof of principles shown in the current F-104G experiments—regarding in-flight laser-based methods. The simplest is imaging of OH chemiluminescence in the UV, yielding the trajectory of the reacting portion of the jet. Alternatively, one could image OH fluorescence obtained by pumping the X -> A transition with a XeCl excimer laser. This would yield both the trajectory of the reacting jet and insight into its interior structure, including interactions between turbulence and chemistry that dictate the burning rate.

Given the availability of aircraft and support at NASA Dryden and the numerous experiments already conducted, proposed, and those yet to be, we can assuredly say that in-flight aero/thermo/fluid dynamic experiments employing sophisticated instrumentation and diagnostics have a bright and promising future.
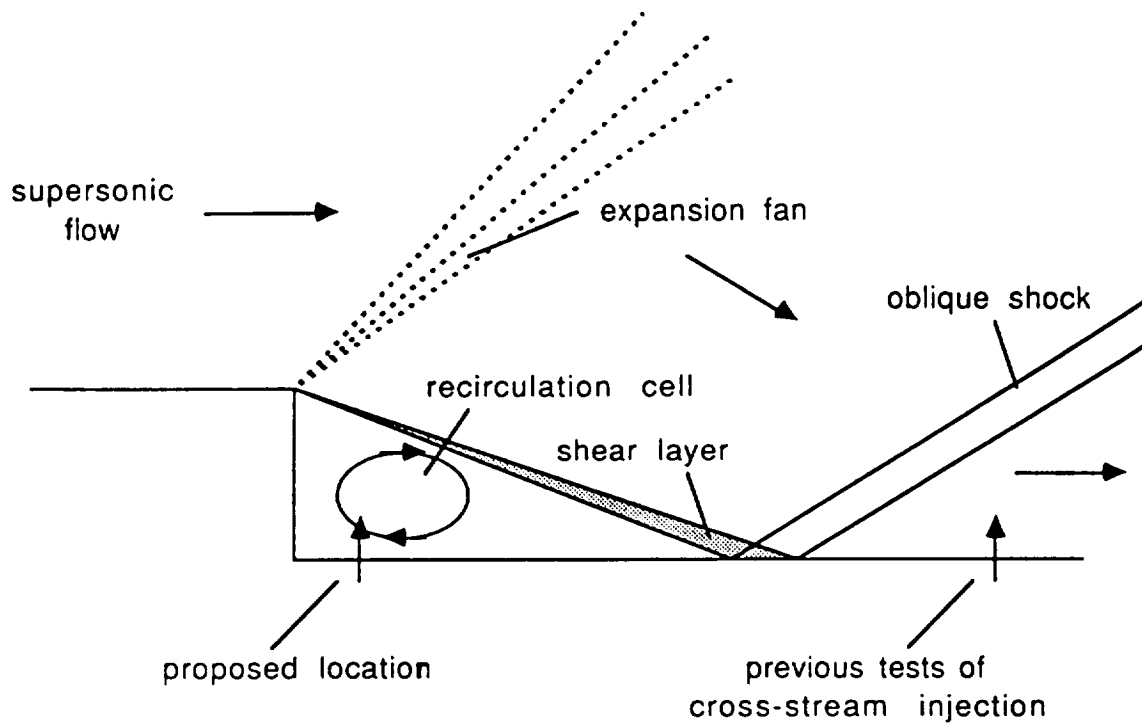
supersonic flow

expansion fan

oblique shock

recirculation cell

shear layer

proposed location

previous tests of cross-stream injection

Figure 5.1   Future Work: Injection Behind a Rearward-Facing Step

ACKNOWLEDGMENTS

APPENDIX 1
MAINTENANCE AND OPERATIONS

The following is a detailed text on proper maintenance procedures necessary to keep the subsystems operational. Various parts referred to can be seen in Figures 2.4–2.10. Critical parts and issues are highlighted for convenience should repairs or maintenance be needed. For reordering information, see the Parts List and Supplier List included as Appendix 2.

Jet Formation Subsystem

The **nitrogen tank** is filled to 3000 psi through a retractable **fill port** at the upper aft end of the ICR. By turning open the **access valve**, nitrogen is allowed to flow through the regulator and into the tank. Filling should be performed by personnel familiar with handling high-pressure gases. Note that pressurizing should be done slowly so that the tank does not heat up excessively, though some warming is expected. **Leaks** can be detected using soapy water injected around threaded or Swagelock connections. Problems with the **valve stem** of the nitrogen tank should be directed to the supplier, Phoenix Distributing. Problems with the tank should be directed to its supplier, NASA Dryden.

The Fisher Scientific **pressure regulator** does not need regular maintenance. It is adjusted using the dial knob in front. If maintenance on any of the three Statham **transducers** is needed, consult NASA Dryden or Schlumberger Industries. Note that they are all connected with AN (not Swagelock) fittings.

The **nitrogen line** leading from the regulator to the nitrogen solenoid valve is the primary component to remove when access to the rest of the jet subsystem under the laser platform is required. Removing the line involves loosening the Swagelock nuts at the line ends and removing the 1/4-20 allen hex screws holding down the solenoid valve. Upon doing this, the higher end of the line will have enough play so that it can be pulled down/out of its fitting. Reinstalling the above is in reverse order, the last item being inserting the line up/in to its fitting. A screwdriver acting as a cantilever against the heater controller mount can assist in reinserting the line.

All **Swagelock connections** should be tightened in accordance with standards outlined in the Swagelock manual. A handy reminder is to tighten the nut 1.25 turns after the nut has been tightened finger tight, assuming it can be finger tightened freely. A Gap Inspection Gage can also be purchased to check proper fitting installation.

The Burkert **nitrogen solenoid** valve is maintenance-free. If it should fail, first check if the maximum inlet pressure has been exceeded (approx. 45 psia), in which case the solution is simply to adjust the regulator to a lower pressure.

The **nitrogen preheater** may need upkeep from time to time. In particular are the electrical feedthroughs and the heating element itself. The **feedthroughs** are susceptible to loosening up when the temperature inside the preheater is too hot, causing the solder joints

59

to melt. To avoid this, make sure there is always a sufficient amount of nitrogen flow (near operating conditions) when the heater is on. If the feedthroughs should fail, higher temperature solder should be applied to the joints. During ground tests where low flow may be necessary, place some wet towels around and under the preheater to draw away excess heat.

The **heating element** core is susceptible to embrittlement, also due to excessive temperatures, caused by insufficient nitrogen flow rates. If the core cracks, it should be replaced (see Parts List). Note that mica sheets, included with a new heating element should be placed inside the preheater; this prevents possible short circuiting should the coils touch the preheater inner surface. Removal/replacement of the element is facilitated by an access hole/bolt (solder-sealed and threaded) on top of the preheater.

The nitrogen and iodine lines are mixed at a stainless-steel **T-branch**. The **flow control orifices** for both gases are installed on this branch. The nitrogen orifice is press fit (and easily removed), whereas the iodine orifice is soldered. [The currently replaced iodine valve by General Valve has a proper orifice size, so that the orifice in the T-branch has been removed.]

The **iodine solenoid valve** needs moderate maintenance due to its high-temperature and corrosive environment. The valve should be checked periodically to ensure iodine condensation is not a problem. Condensation can be prevented by assuring that the valve is always the hottest part of the iodine flow path, especially during cooling times, so that iodine will preferentially condense in the iodine tank or the iodine line, rather than in the valve. Because high temperatures are a potential problem to most solenoid valves, we use a General Valve Series 9 valve, which incorporates a coil rated for 220 °C. [If this solenoid valve fails under high temperatures of around 200 °C, air-actuated bellows valves can be used. Such an option is currently under consideration.]

The **iodine line and tank** are made of stainless steel to handle the corrosive properties of iodine. From time to time, the line and tank should be removed and washed down with acetone, and examined. Doing so will eventually help determine how much iodine is used during test runs, and how much should be added between tests. The Omega cartridge heater inside the iodine tank is made of Incoloy alloy and has a welded, sealed tip. Solder tipped cartridge heaters are not robust enough to combat iodine corrosion and must be avoided.

The **nitrogen/iodine line** from the T-branch to the nozzle is sectioned into two separate lines to facilitate removal if/when necessary. One line is very short and straight, and is easily removed when the T-branch is free. The other line is longer and serpentine, and can be removed by manipulating it under the laser power supply or by removing the forward panel of the ICR.

The **nozzle** is removed by first removing the nozzle mount, and then unscrewing the nozzle off the O-ring face seal fitting. Nozzles of different exit diameter or shape should be machined with the mount in mind to facilitate interchangeability between nozzles.

Fiberglass cloth **insulation** is required on all lines and components that are heated with **heating tape**, both for safety purposes and to prevent heat loss to the surroundings. In some cases, insulation is also needed to prevent adjacent components from being overheated, (e.g. the laser head). Glass wool can be helpful in this application.

Items and parts not mentioned above require no special knowledge of removal or maintenance procedure. A little experience, common sense, and elbow grease will go a long way.

Image Acquisition Subsystem (Camera)

The ITT F4577 intensified **camera** is mounted in the front section of the ICR experimental module. The camera lens and two turning mirrors are located above the camera body. The mirrors are mounted and dismounted easily with allen screws. Care should be taken to ensure the mirrors are properly aligned to provide the correct field of view in the fluorescing plane. Due to space constraints, *it is not possible to insert the ICR into the flight test fixture with the camera installed.* The same applies to *removal* of the ICR from the flight test fixture. After ICR installation, the camera may be inserted as follows. First, make sure the switches at the rear of the camera are configured properly. This is discussed in some detail below. Connect the appropriate coaxial cables to the Video Output and External Gate Input BNCs. Connect the camera cable to the DB25 I/O connector at the rear of the camera. Work the camera carefully into its mount from the nozzle side of the ICR, beginning with the rear of the camera. Installation is completed by securing the camera to its mount by tightening the upper three allen screws on the mount back. The bottom allen screw secures a shim to the camera mounting bracket, and need not be touched. To remove the camera, the above procedure is reversed.

It is very important that the configuration switches located at the rear of the camera be set properly before power is applied. Even momentary operation at ambient light levels with improper settings can permanently damage the costly intensifier tube. Familiarity with the operating principles of the camera (as obtained, for example, by reading its operating manual) is recommended. In particular, operation in the CW gate mode should not be attempted without some forethought.

The proper settings for the present experiment are given in Table 2. Refer to Figure 5 of the camera installation and operation manual to determine the location of the switches. As a safety measure, it is recommended that controls not listed in Table 2 be placed in the full CCW position. This especially applies to the *Gain Control Pot* and the *Width Course Control Switch.*

Table 2. Camera Setup

Control	Position
Gate mode	Ext
Gain mode	Ext
Intensifier mode	Gate

61

Illumination Subsystem (Laser)

The **laser** is powered directly from the aircraft 28 VDC. This modification was installed by the factory. The modification appears to mainly involve installation of a couple of switching power supplies, although it is difficult to be sure (the manufacturer considers all the schematics proprietary, both for the modifications as well as the standard power supply). The 28-V power is supplied to the rear of the power supply via banana plugs. The polarity is arbitrary. We have added a pair of wires, the shorting of which simulates the depression of the laser reset button on the front panel. These wires exit through the back of the case, where they are RTV'd in place. A temporary push button switch shorts the wires, thus activating the laser. The laser power supply is connected to the laser head via three cables; two multiconductor and one coaxial. A coaxial cable must also be connected between sync out BNC at the rear of the power supply and the gate input BNC on the camera.

The **laser power supply** should be set up as specified in Table 3.

Table 3. Laser Setup

Control	Position
110-VAC key	Off & removed
28-VDC key	Inserted & on
110-VAC/28-VDC switch	28 VDC
Feedback	Int
Q- switch	Int
Prelasing	Off
Frequency Range	High
Frequency Pot	Adj for max power (approx. 2 kHz)

As noted in the above table, we have set the laser repetition rate to the maximum power setting (about 2 kHz). In preliminary tests with room light background, this seemed to provide the best signal to noise. However, according to the laser manufacturer (see page 7 of the manual), the highest pulse energy can only be maintained below 1 kHz. To gain full benefit of the gated camera, the pulse energy should really be maximized (not the power, e.g., the product of the pulse energy and repetition rate). Therefore, in high ambient light environments better signal to noise may be obtainable at lower repetition rates. This adjustment can easily be made at the front panel of the power supply.

The **laser head** incorporates a solid state (diode) laser pumping a frequency doubled Nd:YAG laser. A thermoelectric heater/cooler, designed to operate between 0 and 30 °C, is used to maintain the temperature of the doubling crystal. We have made provision for heating the laser head in the event of low ambient temperature. The temperature controller is currently set at 15 °C. This particular controller has an alarm circuit, which is set at 30 °C. The alarm relay could be used to interrupt the power to the laser head heater,

providing some measure of protection against overheating. We have not done this, but we probably should. The laser head contains a mechanical beam shutter, manipulated by twisting the knurled knob at the beam exit aperture. Make sure the shutter is open before trying to run the experiment.

The **associated optics** are aligned in front of the laser head via allen screws mounted from beneath. For fine tuning of the laser sheet position, the turning mirror (inside the optical canopy) is equipped with a multi-axis kinematic mount and tuning screws. The **optical canopy** is affixed with a series of 8-32 aircraft screws. The **canopy window** is actually a 300-mm focal length cylindrical lens that acts to "thin out" the thickness of the laser sheet. It is held in place by epoxy and an aluminum protective plate. Replacement of this window will require removal of the protective plate (a simple and obvious procedure) and melting off of the old epoxy, with the help of a heat gun.

Miscellaneous

Electronic circuitry is detailed in Chapter IV of this paper.

Specific **instruction and/or operating manuals** for the laser, camera, valves, heaters, controllers, conditioners, relays, and thermocouples can be obtained by the manufacturers or suppliers. Individuals at UCLA and NASA responsible for the experiment should have copies of these manuals.

Tables of Connectors and Cables

PIN	FUNCTION	PIN	FUNCTION	COMMENT
			PC EDGE CONNECTOR	
1	+28	A	+28	1-A connected
2	GND	B	GND	2-B connected
3	+15 (from reg)	C		
4	TC 1 (+-5)	D	TC 1 (COM) <-> GND	twisted pair (downlink)
5	TC 2 (+-5)	E	TC 2 (COM) <-> GND	twisted pair (downlink)
6	TC 3 (+-5)	F	TC 3 (COM) <-> GND	twisted pair (downlink)
7	TC 4 (+-5)	H	TC 4 (COM) <-> GND	twisted pair (downlink)
8	LASER RESET (+5)	J	LASER RESET (COIL)	twisted pair (to cockpit)
9	+5 (from reg)	K	CTRL (COM) <-> GND gen/wt + wt/grn	
10	CRTL 1 (+) org/wt	L	CTRL 2 (+) brn/wt	from controllers
11	CTRL 3 (+) blu/wt	M	CTRL 4 (+) wt/org	from controllers (NC to #4)
12	JET HEAT (TTL) wt/brn	N	IODINE LINE HEATER (TTL) wt/blu	
13	EXPT TRIG	P	EXPT TRIG (GND)	twisted pair (to cockpit)
14	VALVE PWR (28 -> 24)	R	CAMERA GATE MONITOR (TTL)	
15	CAMERA EXT GAIN (0-10)	S	CAMERA EXT GAIN (COM) <-> GND	CCW to increase gain
16	CAMERA POWER (+15)	T	CAMERA POWER (COM) <-> GND	
17	LASER RESET	U	LASER RESET	twisted pair (to laser PS)
18		V	VALVE PWR (SWITCHED)	
19		W		
20	110 AC (in)	X	110 AC (in)	
21	JET LINE HTR. 110 AC (switched)	Y	LASER HEAD HTR. 110 AC (switched)	
22	Z	IODINE CELL HTR. 110 AC (switched)		

UNIT	FUNCTION	COMMENTS
CTRL 1	iodine cell heater	logic output to PC board
CTRL 2	iodine line heater	logic output to PC board
CTRL 3	jet line heater	logic output to PC board
CTRL 4	laser head heater	SSR output to heater
TC 1	iodine cell tc	to CTRL1, then SC1
TC 2	iodine valve tc	to CTRL2, then SC2
TC 3	jet line tc	to SC3, then CTRL3
TC 4	jet exit tc	to SC4

DB25 PIN	PC EDGE PIN	FUNCTION	COMMENTS
		CAMERA CABLE	
12	15	intensifier gain (0-10)	white
24	S	intensifier gain (com)	black
13	16	camera power (+15)	red
1/25	T	camera power (com)	green
18	R	intensifier gate (ttl)	brown

APPENDIX 2
SUPPLIER AND PARTS LISTING

SUPPLIER	ADDRESS & PHONE NO.	CONTACT
AB Lasers	4 Craig Road Acton, MA 01720 Tel 508-635-9100 FAX 508-635-9199	Gerhard Marcinkowski (Tech Rep) Joanne Keene (Sales & Marketing)
A. Biederman, Inc.	627 Hazel Street P.O. Box 25003 Glendale, CA 91201-3095 Tel 818-246-8431	Pablo or Dave (Sales)
ADLAS Advanced Design Lasers	Seelandstrasse 67 2400 Lubeck 14 Germany Tel 49-451-3909300 FAX 49-451-3909399	
All Aircraft	6712 Balboa Blvd. Van Nuys, CA (Sherman Way west exit off 405) Tel 818-894-9115	
Analog Devices	3000 W. MacArthur Blvd. Suite 150 Santa Ana, CA 92704 Tel 714-432-5224	Jean (Sales)
Angeles Valve & Fitting	427 S. Victory Blvd. Burbank, CA 91502 Tel 818-846-8201	
B.J. Wolfe Ent.	10760 Burbank Blvd. N. Hollywood, CA 91601 Tel 213-877-5518 Tel 818-984-3754 FAX 818-984-2351	Brad Wolfe (Owner)
Burkert Contromatic Corporation	1091 N. Batavia Street Orange, CA 92667 Tel 714-744-3230 FAX 714-639-4998	Craig Occhiato (Tech Rep)

Crest Industries	26845 Oak Avenue, Unit 15 Santa Clarita, CA 91351 Tel 805-252-6873 FAX 805-252-4658	Richard Hayes (President) Joyce (Sales)
Edmund Scientific	101 E. Gloucester Pike Barrington, NJ 08007-1380 Tel 609-573-6250 FAX 609-573-6295	Steven (Tech Rep)
Fisher Scientific	2761 Walnut Avenue P.O. Box 9800 Tustin, CA 92681 Tel 714-669-4600	
General Valve Corporation	19 Gloria Lane P.O. Box 1333 Fairfield, NJ 07006 Tel 201-575-4844 FAX 201-575-4011	Marie (Sales)
ITT Electro-Optical Products Division	7635 Plantation Rd, NW Roanoke, VA 24019-0065 Tel 703-563-0371 FAX 703-362-7370	Bill Decker (Sales) x4415 Nancy Dowdy (Cust. Service) x4337
McMaster-Carr Supply Company	P.O. Box 54960 Los Angeles, CA 90054-0960 Tel 310-692-5911	
Melles-Griot	1770 Kettering St. Irvine, CA 92714 Tel 714-261-5600 Tel 800-835-2626	Glen Mashburn (Cust Service)
NASA Dryden Flight Research Center	P.O. Box 273 Edwards, CA 93523 Tel 805-258-3716 FAX 805-258-3567 Email: bowers@rigel.dfrf.nasa.gov	Al Bowers
Newport Corp.	1791 Deere Avenue Irvine, CA 92714 Tel 714-863-3144 Tel 800-222-6440	

Omega Engineering, Inc.	1 Omega Drive Box 4047 Stamford, CT 06907 Tel 800-622-2378 Tel 800-872-4328 (heaters)	
Oriel Corporation	P.O. Box 872 250 Long Beach Blvd. Stratford, CT 06497 Tel 203-377-8282 FAX 203-378-2457	
Phoenix Distributors	11711 S. Alameda St. Los Angeles, CA 90059 Tel 213-564-5711 FAX 213-569-4951	Larry Box (Sales)
Samy's Camera	7122 Beverly Blvd. Los Angeles, CA 90036 Tel 213-938-2420 Tel 800-321-4-SAMY FAX 213-937-2919	Louis Friedman (Sales)
Schlumberger Industries; Statham Transducer Div.	2230 Statham Blvd. Oxnard, CA 93033	Mike Moerson
UCLA Engineering Tool Crib	SEAS Machine Shops 1012 Engineering I UCLA Los Angeles, CA 90024 Tel 310-825-2264 Tel 310-825-2186	Dave (tool crib) Rick (electrician) Gene (welder) Ian (machinist) Steve (manager)

ITEM DESCRIPTION	PART NO.	SUPPLIER

The Illumination Subsystem

ITEM DESCRIPTION	PART NO.	SUPPLIER
Laser, Diode pumped Nd:YAG (head and power supply)	DPY321QD	AB Lasers/ADLAS
Cylindrical lens holder	07LHC001	Melles-Griot
Plano-cylindrical precision lens f = −6.35 mm coated on concave surface	01LCN123/001	Melles-Griot
Stock mirror, 1 in. diam. 1/20 λ, BD.1 Dielectric coating, Pyrex	10D20/BD.1	Newport Corp.
Mirror mount, 1 in. × 1 in.	MM-1	Newport Corp.
Plano-cylindrical lens f = 300 mm, 50 mm × 60 mm	01LCP019	Melles-Griot
Flexible Silicone Rubber Heater (for laser head)	SRFG-307/5-P	Omega Engineering

The Image Acquisition Subsystem

ITEM DESCRIPTION	PART NO.	SUPPLIER
Image intensified solid-state video camera	F4577	ITT Electro-Optical Product Division
C-mount adapter		Samy's Camera
Nikkor 28 mm, f 2.8 lens	Ser #328226	Samy's Camera
Vis. band-pass filter 550 nm, FWHM = 40 nm	03F1V044	Melles-Griot
Broadband Int. filter 550 nm, 70 nm bandwidth	57581	Oriel Corp.
Colored glass filter 530 nm, cut-on	59500	Oriel Corp.
Laser line int. filter (Nd:YAG 532)	59040	Oriel Corp.

Precision elliptical flat mirror; enhanced Al coating	B32,135	Edmund Scientific Co.
Mirror mount, 1 in. × 1 in.	MM-1	Newport Corp.
Support holder	VPH-2	Newport Corp.
Square flat mirror 100 mm × 100 mm Protected Al surface	01MFG015	Melles-Griot
Long pass IR filter 550 nm cut-on	59884	Oriel Corp.
Long pass colored glass filter, 550 nm cut-on	59502	Oriel Corp.
Support post	SP-3	Newport Corp.

The Jet Formation Subsystem

Nitrogen cylinder 3000 psi; 6/92 hydro-stated		NASA Dryden
Valve stem, 1 in. NPT, CGA 580		Phoenix Distributing
Pressure regulator two-stage	10-572Q	Fisher Scientific
Iodine cylinder Whitey sample cylinder 75 cc	304L-HDF4-150	Angeles Valve & Fitting
Fiberglass cloth tape 51 mm width × 30.5 m long	01-472B	Fisher Scientific
Nitrogen solenoid valve Type 256	256-A-3/8-F-SS-1/2 -240/60-10-U-H-000	A. Biederman, Inc.
Nitrogen solenoid	S-0256-3004-302-00	Burkert Contromatic Corp.
Iodine solenoid valve Type 255	255-A-1/4-E-SS-1/2 -240/60-U-H-000	A. Biederman, Inc.
Iodine solenoid	S-0255-3004-302-00	Burkert Contromatic Corp.

Iodine solenoid valve (high-temp coil)	Series 9, SS body, Kalrez seat & seal, Normally closed, 20 VDC, 1/8 in. NPT, 0.116 in. orifice	General Valve Corp.
Nitrogen preheater Modified Whitey Sample cylinder, 300 cc	304L-HDF4-300	Angeles Valve & Fitting
Assorted brass & stainless steel fittings		Angeles Valve & Fitting
Stainless steel tubing 1/2 in., 3/8 in., 1/4 in.		UCLA Eng. Tool Crib or McMaster-Carr
Pressure transducers 0-15 psia 0-50 psia 0-5000 psia	Ser. #4214 Ser. #28145 Ser. #10418	NASA Dryden or Schlumberger, Statham Transducer Division
Samox ultra-high temp. heating tapes 1/2 in. × 1/2 in. 1 in. × 2 in.	STH051-020 STH101-020	Omega Engr.
Temperature controller CN76000 series	CN76120-PV	Omega Engr.
Thermocouples, Type E (cement-on)	CO1-E	Omega Engr.
Solid-State relay	SSR240AC10	Omega Engr.
Thermocouple wire, Type E (insulated)	GG-E-30-25	Omega Engr.
Nitrogen fill valve (integral bonnet needle valve)	SS-20VM4-F4	Angeles Valve & Fitting
Leak detector, Snoop	MS-SNOOP-207	Angeles Valve & Fitting
Thermocouple signal conditioner, isolated	2B50A	Analog Devices

Nitrogen heating element 120 V, $\approx$ 8 A	3456K23	McMaster-Carr
DC/DC Converter Power Supply	945	Analog Devices
T/C grounded sheath probe submini; Type E	GEMQSS-040G-6	Omega Engr.
Heat conductive putty 1 gallon	3568K1	McMaster-Carr

Glass fiber insulation sheet
  semi-rigid, 1 in. thick
  foil faced
	9350K1	McMaster-Carr

Transducer connectors (Bendix)	PT06A-10-6SSR	Crest Industries

Iodine cylinder cartridge
  heater, 1/4 in. diam., 5 in. long,
  100 W, Incoloy sheath
	CIR-105/120	Omega Engr.

Miscellaneous & Special Items

Dow Silicone RTV (opaque or grey)	3145	NASA Dryden

Helicoil Repair Kit		McMaster-Carr
4-40	91732A267	
8-32	91732A269	
10-24	91732A311	
1/4-20	91732A312	
Metric M6	91732A062	

Helicoil Screwlock Inserts		McMaster-Carr
4-40 (short)	90296A101	
4-40	90296A102	
8-32 (short)	90296A111	
8-32	90296A112	
10-24	90296A122	
1/4-20 (short)	90296A121	
1/4-20	90296A122	
Metric M6	90296A308	

Helicoil Extracting Tool		McMaster-Carr
3-8(UNC)	90254A310	
10-3/8(UNC)	90254A320	
Wagon, Steer-rite	8354T41	McMaster-Carr
wood deck		
100 deg., 3/8 in. diam., 3-flute	2742A35	McMaster-Carr
countersink, for		
aircraft screws		
Heating element for preheater	3149K31	McMaster-Carr
(lower wattage)		
5 A, 120 V		
Epoxy, 5-minute		UCLA Tool Crib
Aircraft structural screws		All Aircraft or
8-32, various lengths		NASA Dryden
AN fittings (blue)		NASA Dryden
Nitrogen cylinder straps		NASA Dryden
(flight-certified)		

APPENDIX 3
PRELIMINARY ANALYTICAL AND DESIGN CODES

```fortran
      program ftf1
c==================================================================
c This FORTRAN program assists in the design of the jet formation
c subsystem for gaseous transverse jet experiments, to be flown aboard
c NASA Ames/Dryden's F-104G inside its Flight Test Fixture (FTF).
c Here, we have chosen a target Mach number of 1.6 ahead of the FTF
c wedge head.  We seek to determine the pressure and temperature at the
c jet exit as a function of altitude from 2500 ft to 50000 ft.  The
c freestream passes through an oblique shock, an expansion fan, and a
c bow shock prior to reaching the jet exit.
c==================================================================
      external func
      integer k
      real p1(20), rho1(20), T1(20), beta, M1, Mn1, p2(20), rho2(20), T2
     *(20), Mn2, M2, v2, v3, M3, p3(20), rho3(20), T3(20), M4, p4(20), r
     *ho4(20), T4(20), a, b, eps, zero, func, alt(20)
      logical error
c These are the p1, rho1, and T1 values from 2500 to 50000 ft (by 2500).
      data p1/92498.6,84305.4,76710.1,69678.6,63178.3,57178.1,51647.9,46
     *559.0,41883.9,37596.5,33671.6,30085.2,26814.7,23838.2,21144.4,1875
     *0.2,16627.0,14744.3,13074.8,11594.3/
      data rho1/1.13806,1.05572,.978014,.904766,.835786,.770906,.709951,
     *.652754,.599151,.548983,.502093,.458331,.417548,.379602,.340060,.3
     *01554,.267408,.237129,.210278,.186467/
      data T1/283.2,278.2,273.3,268.3,263.4,258.4,253.5,248.5,243.6,238.
     *6,233.7,228.7,223.8,218.8,216.7,216.7,216.7,216.7,216.7,216.7/
c
      open(unit=1, file='dataftf1.out')
c==================================================================
c R E P E T I T I O N   C O N T R O L
c==================================================================
      k = 1
 10   if (k .eq. 1) then
c==================================================================
c I N P U T   P R O M P T
c==================================================================
      print *, 'This program calculates the pressure, density, & tempera
     *ture along the'
      print *, 'wedge-tipped FTF (deflection angle = 12.875) as a functi
     *on of altitude,'
      print *, '{p1(Pa), rho1(kg/m3), T1(K)} at some freestream Mach # {
     *M1} .'
      print *, ' '
      print *, 'Enter the freestream Mach # { >= 1.58 } :'
      read *, M1
      print *, 'Enter the angle "beta" of the oblique shock at this Mach
     * # :'
      read *, beta
c==================================================================
c C A L C U L A T E   P & T   A C R O S S   S H O C K   &   F A N
c==================================================================
      Mn1 = M1*sin(beta*3.14159/180.0)
      j = 0
c The loop below calculates p, rho, & T using all available altitudes.
      do 20 i=1,20
c
      j=j+2500
      print *,'=================================================
     *=============='
      print *, 'The following results are for an altitude (ft) of:', j
```

73

```fortran
      print *,'==================================================
     *=============='
       p2(i) = p1(i)*(1 + 2.0*1.4*(Mn1**2 - 1.0)/(1.4+1.0))
       rho2(i) = rho1(i)*2.4*Mn1**2.0/(0.4*Mn1**2.0 + 2.0)
       T2(i) = T1(i)*p2(i)/p1(i)*(2.0 + (1.4-1.0)*Mn1**2.0)/((1.4+1.0)*Mn
     *1**2.0)
       Mn2 = sqrt((Mn1**2.0 + 2.0/(1.4-1.0))/(2.0*1.4*Mn1**2/(1.4-1.0)-1.
     *0))
       M2 = Mn2/sin((beta-12.875)*3.14159/180.0)
       print *, 'M2 after the oblique shock is:',M2
       print *, 'p2 after the oblique shock is:',p2(i)
       print *, 'rho2 after the oblique shock is:',rho2(i)
       print *, 'T2 after the oblique shock is:',T2(i)
       v2 = (sqrt(2.4/0.4)*atan(sqrt((0.4/2.4)*(M2**2.0-1.0))) - atan(sqr
     *t(M2**2.0-1.0)))*180/3.14159
       print *, ' '
       v3 = 12.875 + v2
c
c Find the M3 corresponding to v3 using the secant zero-finding method.
      if (i .eq. 1) then
         print *, 'To get M3 from v3 (Prandtl-Meyer Function, v), we wil
     *l use the secant method.'
         print *, 'The v3 is:', v3
         print *, 'From the Prandtl-Meyer tables, enter two values for M
     *3:'
         read *, a, b
         print *, 'Enter the desired tolerance:'
         read *, eps
         print *, ' '
         call secant(v3,a,b,eps,func,error,zero)
         if (error) then
            print *, 'The secant method failed for the given inputs...'
         else
            print *, ' '
            print *, 'M3 after the expansion fan is:', zero
            print *, 'The function value there is', func(v3,zero)
         endif
         M3 = zero
      endif
c
      T3(i) = T2(i)*(1.0 + 0.2*M2**2.0)/(1.0 + 0.2*M3**2.0)
      rho3(i) = rho2(i)*(T3(i)/T2(i))**2.5
      p3(i) = p2(i)*(T3(i)/T2(i))**3.5
      print *, 'p3 after the expansion fan is:',p3(i)
      print *, 'rho3 after the expansion fan is:',rho3(i)
      print *, 'T3 after the expansion fan is:',T3(i)
      print *, ' '
c The bow shock in front of the jet can be approximated as a normal
c shock in order to find the crossflow Mach # at the jet exit.
      M4 = sqrt( (1.0 + 0.2*M3**2.0)/(1.4*M3**2.0 - 0.2) )
c The pressure, density, and temperature can be approximated using
c the following Godonov-derived correlations by Heister & Karagozian.
      if (M3 .ge. 1.5) then
         p4(i) = p3(i)*(0.405+0.426*M3**2.0)
      elseif (M3.gt.0.8 .and. M3.lt.1.5) then
           p4(i) = p3(i)*(0.861+0.217*M3**2.0)
        else
           p4(i) = p3(i)
      endif
      if (M3 .ge. 2.0) then
```

```fortran
          rho4(i) = rho3(i)*(0.651+0.805*alog(M3))
       elseif (M3.gt.0.8 .and. M3.lt.2.0) then
          rho4(i) = rho3(i)*(0.964+0.0565*M3**2)
       else
          rho4(i) = rho3(i)
       endif
       T4(i) = p4(i)/(rho4(i)*287)
c=================================================================
c P R I N T     F I N A L     R E S U L T S
c=================================================================
       print *, 'After the normal/bow shock, M4 at the jet exit is:', M4
       print *, 'We now use the Godonov correlations for p4, rho4, & T4.'
       print *, 'p4 at the jet exit is:', p4(i)
       print *, 'rho4 at the jet exit is:', rho4(i)
       print *, 'T4 at the jet exit is:', T4(i)
       print *, ' '
c=================================================================
c W R I T E    R E S U L T S    I N T O    O U T P U T    F I L E
c=================================================================
       write(1,*)j, p4(i), rho4(i), T4(i)
c
 20    continue
c
c Ask the user for repetition with a new freestream Mach #.
       print *, ' '
       print *, 'Enter a "1" to repeat or "0" to end :'
       read *, k
       goto 10
       endif
c
       stop
       end
c
c=================================================================
c F U N C T I O N    func
c=================================================================
       real function func(v3,x)
       real x,v3
       func =(sqrt(2.4/0.4)*atan(sqrt((0.4/2.4)*(x**2.0-1.0))) - atan(sqr
      *t(x**2.0-1.0)))*180/3.14159 - v3
       return
       end
c=================================================================
c S U B R O U T I N E    secant
c=================================================================
       subroutine secant(v3,p1,p2,eps,f,error,zero)
       real p1,p2,x1,x2,xnew,f,eps,f1,f2,zero,abs,v3
       logical error
       x1 = p1
       x2 = p2
       small = 1.0E-4
       error = .false.
       f1 = f(v3,x1)
       f2 = f(v3,x2)
 100   if (abs(f1-f2).gt.eps .and. .not.error) then
          if (abs(f1-f2) .lt. small) then
             error = .true.
          else
             xnew = x2 - f2*(x1-x2)/(f1-f2)
             x1 = x2
```

```
            f1 = f2
            x2 = xnew
            f2 = f(v3,x2)
            print *, 'The current approximation is:', xnew
         endif
         goto 100
      endif
      zero = xnew
      return
      end
c=====================================================================
```

```fortran
      program ftf2
c=================================================================
c This program analyzes the jet subsystem thermodynamics for transverse
c jet experiments aboard NASA Ames/Dryden's F-104G/FTF.
c=================================================================
      real mdot, mdotI2, mw, jetint
c All other variables are real.
c=================================================================
c Prompt the user for the desired conditions at the jet exit.
c=================================================================
      print *, '=================================================
     *===================='
      print *, 'This program calculates the thermodynamics for the jet s
     *ubsystem.'
      print *, '=================================================
     *===================='
      print *, ' '
      print *, 'Enter the gamma and molecular weight of the gaseous jet:
     *'
      read *, g, mw
      print *, 'Enter the desired pressure and temperature of the Mach 1
     * gas jet at '
      print *, '   the jet nozzle exit [Pa, K]: '
      read *, pe, Te
      print *, 'Enter the diameter of the nozzle exit [mm]:'
      read *, de
      print *, 'We will assume a 2:1 area ratio for the converging nozzl
     *e forming the jet.'
      print *, 'This means the Mach # at the nozzle entrance will be 0.3
     *.'
c=================================================================
c Calculate the nozzle entrance conditions for isentropic flow knowing
c the nozzle exit conditions.  Print results.
c=================================================================
      p6 = (1.0+((g-1.0)/2.0)*(0.3)**2.0)**(-g/(g-1.0))*(1.0+((g-1.0)/2.
     *0)*(1.0)**2.0)**(g/(g-1.0))*pe
      T6 = (1.0+((g-1.0)/2.0)*(0.3)**2.0)**(-1.0)*(1.0+((g-1.0)/2.0)*(1.
     *0)**2.0)*Te
      print *, 'The conditions at the nozzle exit (e) are:'
      print *, '   Pressure:   ', pe
      print *, '   Temperature:', Te
      print *, 'The conditions at the nozzle entrance (6) are:'
      print *, '   Pressure:   ', p6
      print *, '   Temperature:', T6
      print *, 'The conditions at points 5, 4, & 2 are determined by poi
     *nt 6.'
      print *, ' '
c=================================================================
c Calculate the heat transfer losses and requirements for the gas, N2
c or He between points 0, 1, and 2.
c=================================================================
      if (g.eq.1.4) then
      print *, 'The pressurized nitrogen upstream undergoes expansion co
     *oling as it expands'
      print *, 'between points 0 and 1.  We assume a Joule-Thompson type
     * cooling process.'
      print *, 'If we take p0 & T0 inside the tank to be 2500psi & 293K,
     * and the p1 to be about 1psi (slightly above p2), we will have a t
     *emperature drop of about 32K.'
      print *, 'The conditions at point 1 are thus:'
```

```fortran
      print *, '    Pressure: (approx.) 101325 Pa'
      print *, '    Temperature:       261 K'
      else
      print *, 'The pressurized helium upstream undergoes no cooling dur
     *ing expansion, T1=T0.'
      endif
      print *, ' '
      print *, 'Enter the temperatures at points 1 & 2:'
      read *, T1, T2
      dT21 = T2 - T1
      print *, 'Enter the spec. ht. at constant pressure for the gas, at
     * 1 atm. [kJ/kg-K] :'
      read *, cp
      rhoe = pe/(8314/mw*Te)
      veloe = sqrt(g*8314/mw*Te)
      areae = 3.14159*(de/1000)**2/4
      mdot = rhoe*veloe*areae
      q12 = mdot*cp*dT21
c Assume pressure between 1 and 2 is near constant & thus equal to p6.
      Qin = 1000*mdot/(p6/(8314/mw*T1))
      Qout = 1000*mdot/(p6/(8314/mw*T2))
c Print heating results.
      print *, 'The mass flowrate of the gas is [kg/s] :', mdot
      print *, 'The q, heat rate [kW], required to heat the gas from T1
     *to T2 is:', q12
      print *, 'The volumetric flow rate [l/s] of the gas into the heate
     *r is:', Qin
      print *, 'The volumetric flow rate [l/s] of the gas out of the hea
     *ter is:', Qout
      print *, ' '
c=====================================================================
c Calculate the I2 into gas mixing conditions.
c=====================================================================
c We choose the I2 volumetric flow rate to be .002 that of the gas
c outgoing volumetric flow rate, giving an I2 seeding of 2000 ppm.
      QI2 = .002*Qout
      rhoI2 = p6/(32.76*T6)
      mdotI2 = rhoI2*QI2/1000
      print *, 'Enter the diameter of the iodine "injector" [mm]:'
      read *, dI2
      areaI2 = 3.14159*(dI2/1000)**2/4
      veloI2 = QI2/1000/areaI2
      p3 = p6 + rhoI2*veloI2**2
      print *, 'The required flow rate [l/s] for the I2 to maintain 2000
     * ppm is:', QI2
      print *, 'The corresponding mass flow rate [kg/s] is:', mdotI2
      print *, 'The corresponding velocity [m/s] through the injector is
     *:', veloI2
      print *, 'The upstream I2 pressure (in a heated tank) should be at
     * least:', p3
      print *, ' '
c=====================================================================
c Calculate the N2 and I2 supply requirements.
c=====================================================================
      print *, 'Enter the jet interval time [s] per run:'
      read *, jetint
      print *, 'Enter the # of runs per flight:'
      read *, runs
      print *, 'Enter the pressure and temperature of the pressurized ga
     *s [si]:'
```

```
      read *, p0, T0
      print *, 'Enter the temperature of the I2 in its heated tank:'
      read *, T3
      run = mdot*jetint
      flight = run*runs
      rho0 = p0/(8314/mw*T0)
      runI2 = mdotI2*jetint
      flightI2 = runI2*runs
      rho3 = p3/(32.76*T3)
c Print results.
      print *, ' '
      print *, 'For each run, we need: gas (kg) :', run
      print *, '                        : I2  (kg) :', runI2
      print *, ' '
      print *, 'For each flight, we need: gas (kg) :', flight
      print *, '                        : I2  (kg) :', flightI2
      volgas = 1000*flight/rho0
      volI2 = 1000*flightI2/rho3
      print *, '                        : gas (l) :', volgas
      print *, '                        : I2  (l) :', volI2
c=================================================================
      stop
      end
```

REFERENCES

Anderson, J.D., *Modern Compressible Flow: With Historical Perspective*, Second Edition, McGraw-Hill Book Company, 1990.

ASME Staff Report, "Propelling the Aerospace Plane," *Mechanical Engineering*, Vol. 108, 1986, p. 32.

Broadwell, J.E. and Breidenthal, R.E., "Structure of Mixing of a Transverse Jet in a Cross Flow," *Journal of Fluid Mechanics*, Vol. 148, 1984, p. 405ff.

Chitsomboon, T., Northam, G.B., Rogers, R.C., and Diskin, G.S., "CFD Prediction of the Reacting Flowfield Inside a Subscale Scramjet Combustor," AIAA Paper No. 88-3259, AIAA/SAE/ASME/ASEE 24th Joint Propulsion Conference, Boston, Massachusetts, July 11–13, 1988.

Csorba, Illes P., "New Technology Enhances Image Acquisition," *Laser Focus World*, January 1990, pp. 149–150.

Csorba, Illes P., "The Generations of Image Tubes," *Optical Engineering Reports*, No. 60, December 1988, pp. 1, 6.

Fletcher, D.G. and McDaniel, J.C., "Laser-Induced Fluorescence Technique for Quantitative Measurements in a Nonreacting Supersonic Combustor," *AIAA Journal*, 1990.

Heister, S.D. and Karagozian, A.R., "Gaseous Jet in Supersonic Crossflow," *AIAA Journal*, Vol. 28, No. 5, 1990(a), pp. 819–827.

Heister, S.D. and Karagozian, A.R., "Vortex Modeling of Gaseous Jets in a Compressible Crossflow," *Journal of Propulsion and Power*, Vol. 6, No. 1, 1990(b), pp. 85–92.

Heister, S.D., Nguyen, T.T. and Karagozian, A.R., "Modeling of Liquid Jets Injected Transversely into a Supersonic Crossflow," *AIAA Journal*, Vol. 27, No. 12, 1989, pp. 1727–1734.

Hultgren, R. et al., *Selected Values of the Thermodynamic Properties of the Elements*, American Society for Metals, Metals Park, Ohio, 1972, pp. 246–251.

Kamotani, Y. and Greber, I., "Experiments on a Turbulent Jet in Cross Flow," *AIAA Journal*, Vol. 10, 1972, p. 1425ff.

Karagozian, A.R., "An Analytical Model for the Vorticity Associated with a Transverse Jet," *AIAA Journal*, Vol. 24, 1986, p. 429ff.

King, P.S., Thomas, R.H., Schetz, J.A., and Billig, F.S., "Combined Tangential-Normal Injection into a Supersonic Flow," *Journal of Propulsion and Power*, Vol. 7, No. 3, 1991, pp. 420–30.

Lee, M.P., McMillin, B.K., Palmer, J.L., and Hanson, R.K., "Planar Fluorescence Imaging of a Transverse Jet in a Supersonic Crossflow," *Journal of Propulsion and Power*, Vol. 8, No. 4, 1992, pp. 729–735.

Le, A.T. and Karagozian, A.R., "Transverse Gaseous Jet Injection Behind a Rearward-Facing Step Into a Supersonic Crossflow," *AIAA Journal* (submitted), 1992.

Manela, J. and Seginer, A., "Jet Penetration Height in Transonic Flow," *AIAA Journal*, Vol. 24, 1986, p. 67.

McDaniel, J.C. and Graves, J., "Laser-Induced Fluorescence Visualization of Transverse Gaseous Injection into a Nonreacting Supersonic Combustor," *Journal of Propulsion and Power*, Vol. 4, 1988, pp. 591–597.

Merzkirch, W., *Flow Visualization*, Academic Press, Inc., London, 1987, pp. 247–254.

Meyer, R.R., "A Unique Flight Test Facility: Description and Results," ICAS Paper 82-5.3.3, 13th ICAS Congress/AIAA Aircraft Systems and Technology Conference, August 1982.

Nguyen, T.T. and Karagozian, A.R., "The Liquid Fuel Jet in Subsonic Crossflow," submitted to *Journal of Propulsion and Power*, 1991.

Northam, G.B. and Anderson, G.Y., "Survey of Supersonic Combustion Research at Langley," AIAA Paper 86-0159, January 1986.

Orth, R.C., Schetz, J.A. and Billig, F.S., "The Interaction and Penetration of Gaseous Jets in Supersonic Flow," NASA CR-1386, p. 1869ff.

Phillips, E.H., "Flight Tests Demonstrate Use of External Burning As Alternative to NASP Wind Tunnel Evaluations," *Aviation Week and Space Technology*, July 27, 1992, pp. 52–53.

Pirello, C.J., Hardin, R.D., Heckart, M.V., and Brown, K.R., "An Inventory of Aeronautical Ground Research Facilities, Volume I—Wind Tunnels," NASA CR-1874, 1971.

Reider, S.B., "Air Breathing Propulsion–Aerospace Highlights 1986," *Aerospace America*, Vol. 24, 1986, p. 32.

Schetz, J.A. and Billig, F.S., "Studies of Scramjet Flowfields," AIAA/SAE/ASME/ASEE 23rd Joint Propulsion Conference, San Diego, California, June 29–July 2, 1987.

Simmons, J.D. and Hougen, J.T., "Atlas of the I_2 Spectrum from 19,000 to 18,000 cm^{-1}," *J. Res. Nat. Bureau Stds.*, Vol. 81A, 1977, p. 25ff.

Sitz, G.O. and Farrow, R.L., "Use of an Fluorescence Cell to Monitor Single-Mode Operation of an Injection Seeded YAG Laser," private communication, 1990.

Uenishi, K. and Rogers, R.C., "Three Dimensional Computation of Mixing of Transverse Injector in a Ducted Supersonic Airstream," AIAA Paper 86-1423, June 1986.

Urie, D. and Lux, D., "Lockheed SR-71 Supersonic/Hypersonic Research Facility, Researcher's Handbook," Vols. 1 and 2, Lockheed Advanced Development Company, Sunland, California, 1992.

United States Committee on Extension of the Standard Atmosphere, *U.S. Standard Atmosphere, 1976*, National Oceanic and Atmospheric Administration, Washington DC, 1976.

Weast, R.C., *Handbook of Chemistry and Physics*, CRC Press, Boca Raton, Florida, 1991.

Zukoski, E.E. and Spaid, F.W., "Secondary Injection of Gases into a Supersonic Flow," *AIAA Journal*, Vol. 2, 1964, p. 1689ff.

REPORT DOCUMENTATION PAGE

Public reporting burden for this collection of information is estimated to average 1 hour per response, including the time for reviewing instructions, searching existing data sources, gathering and maintaining the data needed, and completing and reviewing the collection of information. Send comments regarding this burden estimate or any other aspect of this collection of information, including suggestions for reducing this burden, to Washington Headquarters Services, Directorate for Information Operations and Reports, 1215 Jefferson Davis Highway, Suite 1204, Arlington, VA 22202-4302, and to the Office of Management and Budget, Paperwork Reduction Project (0704-0188), Washington, DC 20503.

1. AGENCY USE ONLY (Leave blank)	2. REPORT DATE November 1994	3. REPORT TYPE AND DATES COVERED Contractor Report

4. TITLE AND SUBTITLE

In-Flight Imaging of Transverse Gas Jets Injected Into Transonic and Supersonic Crossflows: Design and Development

5. FUNDING NUMBERS

WU 505-68-53
NCC 2-374

6. AUTHOR(S)

Kon-Sheng Charles Wang, currently employed by PRC, Inc., Edwards, CA 93523

7. PERFORMING ORGANIZATION NAME(S) AND ADDRESS(ES)

Mechanical, Aerospace, and Nuclear Engineering Department
School of Engineering and Applied Science
University of California, Los Angeles
Los Angeles, CA 90024

8. PERFORMING ORGANIZATION REPORT NUMBER

H-2027

9. SPONSORING/MONOTORING AGENCY NAME(S) AND ADDRESS(ES)

National Aeronautics and Space Administration
Washington, DC 20546-0001

10. SPONSORING/MONITORING AGENCY REPORT NUMBER

NASA CR-186031

11. SUPPLEMENTARY NOTES

Tech monitors Dr. Kenneth W. Iliff and Albion H. Bowers. This report was originally prepared as a project submitted in partial satisfaction of the requirements for the degree Master of Science in Mechanical Engineering at University of California, Los Angeles, March 1993.

12a. DISTRIBUTION/AVAILABILITY STATEMENT

Unclassified—Unlimited
Subject Category 02, 34

12b. DISTRIBUTION CODE

13. ABSTRACT (Maximum 200 words)

The design and development of an airborne flight-test experiment to study nonreacting gas jets injected transversely into transonic and supersonic crossflows is presented. Free-stream/crossflow Mach numbers range from 0.8 to 2.0. Planar laser-induced fluorescence (PLIF) of an iodine-seeded nitrogen jet is used to visualize the jet flow. Time-dependent images are obtained with a high-speed intensified video camera synchronized to the laser pulse rate. The entire experimental assembly is configured compactly inside a unique flight-test-fixture (FTF) mounted under the fuselage of the F-104G research aircraft, which serves as a "flying wind tunnel" at NASA Dryden Flight Research Center. The aircraft is flown at predetermined speeds and altitudes to permit a perfectly expanded (or slightly underexpanded) gas jet to form just outside the FTF at each free-stream Mach number. Recorded gas jet images are then digitized to allow analysis of jet trajectory, spreading, and mixing characteristics. Comparisons will be made with analytical and numerical predictions. (Results presented in AIAA CP-95-0516). This study shows the viability of applying highly sophisticated ground-based flow diagnostic techniques to flight-test vehicle platforms that can achieve a wide range of thermo/fluid dynamic conditions. Realistic flow environments, high enthalpies, unconstrained flow-fields, and moderate operating costs are also realized, in contrast to traditional wind-tunnel testing.

14. SUBJECT TERMS

F-104; Flight test; Flight test fixture; Flow visualization; Imaging; Injection; Nd: YAG laser; Planar laser-induced fluorescence (PLIF); Supersonic; Transonic; Transverse jet

15. NUMBER OF PAGES
85

16. PRICE CODE
AO5

17. SECURITY CLASSIFICATION OF REPORT Unclassified	18. SECURITY CLASSIFICATION OF THIS PAGE Unclassified	19. SECURITY CLASSIFICATION OF ABSTRACT Unclassified	20. LIMITATION OF ABSTRACT Unlimited

NSN 7540-01-280-5500 *For sale by the National Technical Information Service, Springfield, Virginia 22161-2171*

Standard Form 298 (Rev. 2-89)
Prescribed by ANSI Std. Z39-18
298-102